Calcareous nannofossils and paleoclimatic evolution across the Eocene-Oligocene transition at IODP Site U1509, Tasman Sea, Southwest Pacific Ocean

A. Viganò[1,2], E. Dallanave[3], L. Alegret[4], T. Westerhold[5], R. Sutherland[6], G. R. Dickens[7], C. Newsam[8], and C. Agnini[1]

[1]Dipartimento di Geoscienze, Università di Padova, Padova, Italy
[2]Dipartimento di Ingegneria Civile, Edile e Ambientale – ICEA, Università di Padova, Padova, Italy
[3]Faculty of Geosciences, University of Bremen, Bremen, Germany
[4]Departamento de Ciencias de la Tierra & IUCA, Universidad de Zaragoza, Zaragoza, Spain
[5]Center for Marine Environmental Sciences (MARUM), University of Bremen, Bremen, Germany
[6]School of Geography, Environment and Earth Sciences, Victoria University of Wellington, Wellington, New Zealand
[7]School of Natural Science, Trinity College Dublin, College Green, Dublin, Ireland
[8]Network Stratigraphic Consulting Ltd., Harvest House, Cranborne Road, Potters Bar, EN6 3JF, UK

Corresponding author: Allyson Viganò, allyson.vigano@unipd.it

Key Points

- Significant changes in calcareous nannofossil assemblages occurred at the onset of the Eocene-Oligocene transition (EOT; ~34 Ma)
- Calcareous nannofossil diversity decreased during the EOT and warm-oligotrophic taxa were replaced by cold-eutrophic taxa
- Increased paleoproductivity and surface ocean cooling are inferred from the calcareous nannofossil assemblage

Abstract

The Eocene-Oligocene transition (EOT; ~34 Ma) was one of the most prominent global cooling events of the Cenozoic, coincident with the emergence of continental-scale ice-sheets on Antarctica. Calcareous nannoplankton experienced significant assemblage turnover at a time of long-term surface ocean cooling and trophic conditions, suggesting cause-effect relationships between Antarctic glaciation, broader climate changes, and the response of phytoplankton communities. To better evaluate the timing and nature of these relationships, we generated calcareous nannofossil and geochemical datasets ($\delta^{18}O$, $\delta^{13}C$ and $\%CaCO_3$) over a ~5 Myr stratigraphic interval recovered across the EOT from IODP Site U1509 in the Tasman Sea, South Pacific Ocean. Based on trends observed in the calcareous nannofossil assemblages, there was an overall decline of warm-oligotrophic communities, with a shift toward taxa better adapted to cooler more eutrophic conditions. Assemblage changes indicate four distinct phases caused by temperature decrease and variations in paleocurrents: late Eocene warm-oligotrophic phase, precursor diversity-decrease phase, early Oligocene cold-eutrophic phase, and a steady-state cosmopolitan phase. The most prominent shift in the assemblages occurred during the ~550 kyr-long *precursor diversity-decrease phase*, which has relatively high bulk $\delta^{18}O$ and $\%CaCO_3$ values, and predates the phase of maximum glacial expansion (Earliest Oligocene Glacial Maximum – EOGM).

Plain Language Summary

Around 34 Ma, Earth experienced a major glaciation in the southern hemisphere, leading to the formation of permanent continental-scale ice-sheets on Antarctica. The Antarctic glaciation is supposed to have been triggered by a gradual decline of carbon dioxide with tectonic changes playing a secondary role. The separation of Antarctica from Australia and South America, and thus the development of the cold Antarctic Circumpolar Current, may have further intensified the conditions necessary for glacial expansion. This new scenario had profound consequences on climate, with direct effects on the global oceans and marine biota. In the past decades, geoscientists have tried to understand the glacial, tectonic and climatic history of Antarctica, but many questions remain unresolved. In particular, what were the impacts on the oceans in key areas between the Southern Ocean (high-latitudes) and the Equator (low-latitudes), such as the Tasman Sea? We use changes observed in the fossil record of calcifying unicellular algae (calcareous nannofossils) and stable oxygen and carbon isotopes to reconstruct the past surface-ocean evolution of this area. Our results suggest that biological productivity increased as cooler surface-water conditions developed in the Tasman Sea. This was likely driven by invigorated northward-moving nutrient-rich bottom-waters formed in the colder circum-Antarctic area.

1 Introduction

The Eocene–Oligocene transition (EOT, ~34 Ma) was a major change in Earth surface systems characterized by a decrease in global temperatures and large-scale glaciation of Antarctica (Lear et al., 2000; Pearson et al., 2009; Zachos et al., 1996; 2001). The EOT is associated with significant changes in fundamental components of the Earth's system, including sea level, atmospheric CO_2, orbital configuration, land to sea ratio, continental weathering rates, ocean chemistry, circulation and productivity, as well as changes in the role of many positive climate feedbacks, which triggered transient and permanent modifications in marine and terrestrial fauna and flora (e.g. Coxall & Pearson, 2007; Coxall & Wilson, 2011; Hutchinson et al, 2021). During the EOT, a significant paleoceanographic change occurred, both in the Equatorial Pacific Ocean and Southern Atlantic Ocean, leading to a deepening of the carbonate compensation depth (CCD) by more than 1 km (Coxall et al., 2005; Coxall & Pearson, 2007; Pälike et al., 2012; Taylor et al., 2023), which resulted in increased exchange of carbonate from shallow waters to the deep-sea domain.

As evident from benthic foraminiferal stable oxygen isotope ($\delta^{18}O$) records, the transition from late Eocene warmhouse to early Oligocene coolhouse conditions occurred in two prominent orbitally-paced increases in $\delta^{18}O$ that reflect a combination of deep ocean cooling and increased continental ice volume (Coxall & Pearson, 2007). Records such as Mg/Ca of benthic foraminifera and the distribution patterns of temperature sensitive dinoflagellates indicate that most of the cooling (~2°C; Lear et al., 2008) occurred during the first step (Step 1), whereas the second step, named the "earliest Oligocene oxygen isotope step" (EOIS, Hutchinson et al., 2021), recorded a major increase in Antarctic ice volume (Houben et al., 2012; Lear et al., 2008; Haiblen et al., 2019). By definition, the start of the EOT (34.50 Ma; Viganò et al., 2024a), which comprises Step 1 and the EOIS, is marked by the extinction of calcareous nannofossil *Discoaster saipanensis* (Hutchinson et al., 2021). Close to the start of the EOT, a transient interval of more positive $\delta^{18}O$ values, named "Late Eocene

Event" (LEE), is observed in some records and interpreted as a transient cooling and/or glaciation (Hutchinson et al., 2021). The end of the EOT is marked by the top of EOIS (33.66 Ma; Viganò et al., 2024a) and the onset of the earliest Oligocene Glacial Maximum (EOGM), an interval of positive $\delta^{18}O$ values that corresponds with Chron C13n and is interpreted to reflect the onset of continental-scale ice sheets on Antarctica (Coxall et al., 2005; Coxall & Pearson, 2007; Hutchinson et al., 2021; Liu et al., 2004; Miller et al., 1991; Zachos et al., 1996).

Two groups of hypotheses exist to explain the onset and development of Antarctic ice sheets: (1) "the ocean-gateway hypothesis" and (2) "the CO_2 hypothesis". The "ocean-gateway hypothesis", first proposed in the late 1970's, suggests that the opening of Southern Ocean gateways (Exon, Kennet, Malone et al. 2001; Hodel et al., 2022, Livermore et al., 2007; Scher et al., 2015) allowed for a rapid intensification of the Antarctic Circumpolar Current (ACC), which reduced poleward heat flux and thermally isolated Antarctica (Kennett, 1977; Sijp et al., 2004). Subsequent modelling and proxy studies suggest that a global decline in atmospheric CO_2 drove global cooling and ice sheet growth at the EOT (Anagnostou et al., 2016; DeConto & Pollard, 2003; Pagani et al., 2011; Pearson et al., 2009; Zachos & Kump, 2005), with ice-sheet feedbacks and changes in paleoceanography playing a secondary role (Hutchinson et al., 2021; Sauermilch et al., 2021).

In addition to the information derived from geochemical proxies, fundamental insights on the paleoclimatic and paleoceanographic evolution during the late Eocene – early Oligocene come from the spatiotemporal distribution and abundances of calcareous nannofossils, mainly consisting of the fossil tests of coccolithophores (Agnini et al., 2017). In modern oceans, haptophyte algae are important primary producers of organic and inorganic carbon (Rost & Riebesell, 2004). These extremely abundant single-celled planktonic algae form a calcareous test (coccosphere) composed of small (1-30 μm) calcite plates (Perch-Nielsen, 1985). In virtue of their peculiar biological/physiological traits, calcareous nannofossils preserved in ocean sediments are sensitive indicators of past oceanographic and climatic changes to the marine photic zone. Relatively few studies have documented the calcareous nannofossil turnover during the late Eocene to early Oligocene interval (Bordiga et al., 2015; Dunkley Jones et al., 2008; Fioroni et al., 2015; Jones et al., 2019; Persico & Villa, 2004; Villa et al., 2008, 2014, 2021). This knowledge gap partly arises because deep sea sedimentary sequences across this time interval often contain condensed sections that result from significant changes in calcium carbonate preservation.

The shift from the late Eocene warmhouse to the coolhouse climate state of the EOT was accompanied by a decrease in nannofossil diversity that reached a minimum in the early Oligocene (Bown et al., 2004), coinciding with the lowest rates of nannoplankton evolution of the entire Paleogene (Haq, 1973). This diversity decline has traditionally been interpreted to reflect global cooling (Aubry, 1992). The mechanism by which global cooling induces calcareous nannofossil global diversity decline can be explained considering 1) latitudinal (thermal) differentiation between sub-polar and equatorial regions, 2) inter-specific displacement and/or 3) a combination of these factors. In the first scenario, strong latitudinal thermal gradients may have hindered the formation of ecological refugia, thereby contributing to a decrease in diversity. In the second case, the competition between diatoms and coccolithophores likely prevented coccolithophore diversification at higher latitudes, where diatoms emerged as the main phytoplankton group (Bown et al., 2004; Falkowski et

al., 2004; Spencer-Cervato, 1999). The competitive advantage of diatoms leading to diversification over coccolithophores may lie in their ability to cope with increased turbulence and nutrient supply in the upper ocean, conditions that usually characterize glacial periods (Iglesias-Rodríguez et al., 2002; Tozzi et al., 2004). These conditions, together with the absence of ecological refugia, may have contributed to the observed global decrease in calcareous nannofossils during this time.

A complementary explanation for the nannoplankton diversity decline is the nutrient-controlled contraction of the oceanic trophic resource continuum (TRC) resulting from enhanced eutrophic conditions (Hallock, 1987). The sustained eutrophication, although temporary (Coxall et al., 2011), and decreased temperatures during this interval are considered the possible forcing factors for evolutionary turnover and sequential extinctions observed among calcareous nannoplankton (e.g. Aubry, 1992). The long-term decrease in diversity of calcareous nannofossils is mainly related to an increase in the extinction rates during the late Eocene, which became more intense towards the Eocene-Oligocene boundary (EOB) indicating an increase in an environmental pressure, such as a change in ocean thermal structure and/or increased nutrient availability (e.g. Aubry, 1992; Bown et al. 2004).

At present, our understanding of the paleoceanographic evolution of the Tasman Sea and the calcareous nannofossil response during the EOT is limited. The study of this part of the Pacific Ocean is particularly relevant for at least three reasons: 1) it stands as one of the rare sites in the Southwest Pacific characterized by near continuous deposition that remains unaffected by the Marshall unconformity (e.g. Carter, 1985; Carter et al., 2004; Carter & Landis, 1972); 2) it lies in a critical position between equatorial and subantarctic ocean currents (Sutherland et al., 2022); 3) it represents an ideal case study, embodying open ocean sediment deposition with a well-established chronology, that is advantageous to facilitate correlation across extensive geographic regions (Viganò et al., 2024a) and to potentially infer the impact of the opening of the Tasman Gateway (TG) and the early establishment of the Antarctic Circumpolar Current (ACC) on marine biota. Here we present highly resolved calcareous nannofossil and geochemical (bulk $\delta^{13}C$, bulk $\delta^{18}O$, $\%CaCO_3$) records from International Ocean Discovery Program (IODP) Site U1509 (Sutherland et al., 2019), spanning from the late Eocene to the early Oligocene. We analyze changes in the diversity and abundance of the calcareous nannofossil assemblages to reconstruct the local paleoclimatic evolution and connections with Antarctic glaciation and regional paleoceanographic changes. Records generated at Site U1509 provide new insights into how calcareous phytoplankton reacted to the onset of global coolhouse conditions, and contribute to a better understanding of this transition in a key area.

2 Material and methods

2.1 Paleogene marine sedimentary records in the Tasman Sea and IODP Site U1509

The Tasman Sea lies between Australia, New Caledonia and New Zealand (Figure 1), and formed when Zealandia rifted from Australia and Antarctica between the late Cretaceous and early Eocene, about 83 to 53 Ma (Gaina et al., 1998; Hu et al., 2022; Sutherland et al., 2017). Since its inception, sediments, mostly marine, have accumulated on the underlying seafloor. The seafloor of the Tasman Sea area has a complex bathymetry

that includes prominent rises and basins, largely shaped during the initiation of the Tonga-Kermadec subduction zone (Dallanave et al., 2020; Sutherland et al., 2020).

Initial drilling in the region encountered major hiatuses of variable durations from the late Eocene to early Oligocene (Moore et al., 1978) that are associated with the widespread regional Marshall unconformity (e.g. Carter, 1985; Fulthorpe et al., 1996). These hiatuses traditionally have been interpreted to reflect enhanced seafloor erosion caused by intensification of bottom currents during the progressive opening of gateways for the Southern Ocean and the Antarctic glaciation (Close et al., 2009; Sauermilch et al., 2019; Houben et al., 2019; Kennett et al., 1972, 1975a). Extensive seismic studies across the Tasman Sea (Dallanave et al., 2020, 2022; Etienne et al., 2018; Sutherland et al., 2017) now suggest that these unconformities relate to major vertical motions of the seafloor caused by tectonism.

Site U1509 (34°39.13'S, 165°49.66'E) (Figure 1) was drilled at 2911 m water depth in the Tasman Sea during IODP Expedition 371, where the northeast base of Lord Howe Rise converges with the west margin of New Caledonia Trough (NCT) (Sutherland et al., 2019). The estimated paleodepth for this site is lower bathyal (2000 m) during the upper Eocene and slightly deeper (abyssal) during the Oligocene (Sutherland et al., 2019, 2022).

The 690 m thick sedimentary sequence recovered at Site U1509 via rotary drilling (Hole U1509A) can be divided into two lithostratigraphic units (Sutherland, Dickens, Blum et al., 2019). Lithostratigraphic Unit I (0 - 414.57 m CSF-A) consists of ~415 m of Pleistocene to upper Paleocene calcareous ooze, chalk, and limestone, and Lithostratigraphic Unit II (414.57 - 689.68 m CSF-A) consists of ~275 m of Paleocene to Upper Cretaceous claystone. Three subunits are recognized in Lithostratigraphic Unit I. Subunit Ia (0 - 99.60 m CSF-A) is ~100 m-thick and mainly consists of Pliocene to late Oligocene calcareous ooze and chalk with varying foraminifera abundances. Subunit Ib (99.60 - 139.28 m CSF-A) is an upper to lower Oligocene greenish grey calcareous chalk, with abundant nannofossils and common to abundant foraminifera (~40 m). Subunit Ic (139.28 - 414.57 m CSF-A) consists of ~275 m of lower Oligocene to upper Paleocene calcareous chalk and limestone with varying amounts of siliceous microfossils and chert nodules (Sutherland et al., 2019), and it frames the current study. Here we investigated the 183.30 m to 267.30 m interval of Subunit Ic, where depths are expressed in meters CSF-A (see https://www.iodp.org/policies-and-guidelines for depth conventions). This depth interval has a revised age model (Viganò et al., 2024a) that is calibrated to the Geological Time Scale 2020 (GTS20; Gradstein et al., 2020), and generally agrees with shipboard interpretations (Sutherland et al., 2019), but with higher biostratigraphic and magnetostratigraphic resolution. Deposition of this depth interval occurred between the late Eocene and early Oligocene (35.29 to 30.57 Ma). Stratigraphically, the EOT lies between 256.96 m (extinction of *Discoaster saipanensis*) and 246.75 m (top of EOIS) (Viganò et al., 2024a).

Contrary to other locations in the Southwest Pacific, Site U1509 documents a relatively expanded record of the EOT with an average linear sedimentation rate of ~2 cm/kyr; although some recovery gaps are present, they are particularly notable during the early Oligocene (Sutherland et al., 2019; Viganò et al., 2024a). Study of the EOT at this site is thus a unique opportunity for two important reasons: (1) the stratigraphic continuity, and (2) the subtropical location of Site U1509 (~45° S) close to the sub-Antarctic/Antarctic area where the glaciation took place.

192 **2.1.1 Present-day oceanography**

193 At present the oceanography of the study area is influenced by the Antarctic bottom water and the shallow
194 wind-driven East Australian Current (EAC) (Ridgway & Dunn, 2003; Sutherland et al., 2018), which flows
195 along eastern Australia between ca. 18°S and 32°S (Oke, Roughan, et al., 2019), with seasonal variations in
196 strength in response to changes in basin-scale winds (Chiswell et al., 1997). At about 32°S, part of these
197 vortexes propagates into the central Tasman Sea, giving rise to the Tasman Front (TF) (Chiswell et al., 2015;
198 Sutherland et al., 2022) and the Subtropical Front (STF), which pass south of New Zealand (Bostock et al.,
199 2015). The TF represents a surface thermal boundary that periodically moves from north to south, located
200 between eastern Australia and northern New Zealand at 31°–36°S latitude (Oke, Pilo, et al., 2019; Oke,
201 Roughan, et al., 2019).

202 The STF is instead a distinctive surface-water mass present in the Indian, Pacific, and Atlantic oceans
203 generally below 40°S (Hamilton, 2006) and characterized by high primary productivity (Bostock et al., 2015
204 and references herein). The STF represents a dynamic boundary where warm subtropical waters mix with
205 cooler and macronutrient-rich subantarctic waters (Hamilton, 2006; Bostock et al., 2013). Further south, two
206 main circumpolar fronts constitute the ACC: the Subantarctic and Polar Fronts (Rintoul, Hughes, & Olbers,
207 2001).

208

209 **2.1.2 EOT paleogeography and paleocirculation**

210 The late Eocene – early Oligocene paleolatitude for the northern Zealandia Site U1509 is estimated to be
211 ~44–45°S (Dallanave et al., 2022), which is considerably further south than its present-day latitude,
212 approximately at 34.65°S. This is a result of extensive tectonic activities that led to the northward movement
213 of Australia and its separation from Antarctica since the late Eocene (e.g. Cande & Stock, 2004).
214 Approximately at the same time a major reconfiguration of basin and ridge topography occurred within the
215 Tasman Sea area, with the permanent subsidence (>2000 m) of the NCT caused by subduction initiation of the
216 Australia-Pacific convergent plate boundary (Sutherland et al., 2010).

217 At higher latitudes, as the buildup of ice sheets on east Antarctica began (e.g. Zachos et al., 1994) and the
218 opening of the TG occurred, cool surface waters developed south of the proto-STF (pSTF) as part of a
219 developing early-ACC (Hodel et al., 2022; Nelson & Cooke, 2001; Sauermilch et al., 2021), possibly reaching
220 both southern Australia and New Zealand (Kamp et al., 1990). In the latest Eocene, there is evidence of a gyre
221 known as the proto-Ross Gyre (pRG) in the Pacific sector of the Southern Ocean (Exon, Kennett, Malone et
222 al., 2000; Huber et al., 2004; Stickley et al., 2004), while in the Atlantic sector of the Southern Ocean, a proto-
223 Weddell Gyre (pWG) existed even earlier (Vernet et al., 2019) (Figure 1). The EAC, originated from tropical-
224 equatorial currents in the Indian Ocean and from the South Pacific Gyre (SPG), was likely the source of warm
225 waters bathing the Tasman Sea and the Campbell Plateau (Hodel et al., 2022). The opening of the TG in the
226 late Eocene allowed cool high-latitude Indian Ocean waters to mix with warmer southward-flowing subtropical
227 waters of the SPG (Murphy et al., 1986) (Figure 1).

228

2.2 Calcareous nannofossils data

A total of 124 tooth-pick samples were prepared for calcareous nannofossil assemblage analysis. The average sampling resolution is every 66 cm, increasing to ca. 33 cm across the EOT. Samples were prepared following the standard procedure for smear slide preparation (Bown & Young, 1998) and then analyzed using a Zeiss transmitted light microscope (LM) with a 1250× magnification.

Relative abundance patterns (%) of the total assemblage were obtained counting at least 300 specimens per sample. The taxonomy follows that presented by Aubry (1984, 1988, 1989), Perch-Nielsen (1985), Bown (2005), Bown and Dunkley Jones (2012), and Newsam et al. (2017), except for *Dictyococcites* and *Reticulofenestra* for which we use the taxonomy expressed by Agnini et al. (2014). Key calcareous nannofossil datums can be placed into the biostratigraphic frame using three different Cenozoic zonation schemes, NP (Martini, 1971), CP (Okada & Bukry, 1980), and CN of Agnini et al. (2014). The taxonomy of reticulofenestrids is not well constrained due to the heterogeneity of this group (Young, 1990). We assign broadly elliptical/subcircular coccoliths characterized by a faintly visible or imperceptible net in the central area to *Reticulofenestra*, and elliptical forms with a relatively solid central plug closing the central area to *Dictyococcites* (e.g. Backman, 1980; Perch-Nielsen, 1985; Haq, 1971; Young, 1990). The comprehensive discussion of the calcareous nannofossil biohorizons used in these schemes and their ages at Site U1509 are discussed by Viganò et al. (2024a).

Principal component analysis (PCA) was performed on the most abundant calcareous nannofossil taxa (%) of the assemblage using the statistical software PAST (PAleontological STatistic; Hammer et al., 2001). PCA is a multivariate statistical technique that reduces the dimensionality of large data sets so that the variance is explained by a small number of principal components (PCs; Harper, 1999). The fundamental concept behind PCA is to enhance the interpretability of large calcareous nannofossil datasets by reducing their variability along PCs. This helps identify the major loading taxa and evaluate environmental factors affecting changes in the calcareous nannofossil assemblage. For this analysis, we considered the following 15 taxa: *Chiasmolithus, Clausicoccus, Coccolithus, Cyclicargolithus, Dictyococcites, Discoaster, Ericsonia, Isthmolithus, Lanternithus, Reticulofenestra, Sphenolithus, Zygrablithus, Helicosphaera, Cribrocentrum, Blackites*. These taxa comprise 98% to 100% of the assemblage, excluding "Reworking" (reworked specimens) and "Others" (genera with extremely low abundances).

We also conducted an additional PCA focused solely on placoliths to assess their specific contribution during the EOT. This supplementary analysis is particularly significant since placoliths dominate the nannofossil assemblage at this site (86-98% of the total assemblage), thus potentially providing additional insights beyond those obtained from the PCA on the entire assemblage. This analysis involved the following 18 taxa: *Cribrocentrum, Chiasmolithus, Clausicoccus, Coccolithus pelagicus* (6-13 μm), *Cyclicargolithus floridanus, Dictyococcites* (<4 μm), *Dictyococcites* (4-10 μm), *D. bisectus* (>10 μm), *D.* cf. *D. bisectus* (<10 μm), *D.* cf. *D. filewiczii, D. filewiczii, Dictyococcites hesslandii*, *Ericsonia formosa*, *Reticulofenestra* (<4 μm), *Reticulofenestra* (4-10 μm), *Reticulofenestra* (10-14 μm), *Reticulofenestra daviesii*, *Reticulofenestra umbilicus* (>14 μm).

2.3 Paleoecology and diversity indices

Calcareous nannofossils are considered excellent paleoenvironmental proxies and paleoceanographic indicators, due to their broad geographic distribution and sensitivity to paleoenvironmental parameters (e.g., Aubry, 1992; Bordiga et al., 2015; Bown, 1998; Dunkley Jones et al., 2008; Persico & Villa, 2004; Villa et al., 2008; 2021; Wei & Wise, 1990). Key EOT calcareous nannofossil taxa were grouped according to similar paleoecological traits, such as preference for warm-water oligotrophic and cold-water eutrophic conditions. We considered taxa with firmly established ecological affinities. These studies relied on both relative changes in the calcareous nannofossil assemblage and comparisons with various geochemical and paleoenvironmental proxies. In particular, discoasters (e.g., *D. saipanensis* and *D. barbadiensis*) are considered warm-water oligotrophs that are common in abundance at low-middle latitudes (Villa et al., 2008; Wei & Wise, 1990) and *Ericsonia formosa* displays a clear preference for low-middle latitudes and it usually thrives in warm waters (Monechi et al., 2000; Wei & Wise, 1990) and oligotrophic environments (Bralower, 2002; Tremolada & Bralower, 2004; Villa et al., 2008). On this basis, we grouped these taxa as warm-oligotrophic water indicators. Among the cold-eutrophic group, we included *Reticulofenestra daviesii*, *Chiasmolithus* and *Clausicoccus subdistichus* group. The species *R. daviesii* is particularly abundant at high latitudes and considered as a cold-eutrophic taxon (Fioroni et al., 2015; Monechi et al., 2000; Persico & Villa, 2004; Villa et al., 2008; 2014), although Bordiga et al. (2017) proposed that this species may exhibit a more adaptable and tolerant behavior. The genus *Chiasmolithus* is well-established as a cold-water taxon (Bukry, 1973; Persico & Villa, 2008; Villa et al., 2014; Wei & Wise, 1990), possibly adapted to moderate to high nutrients environments (Aubry, 1992; 1998; Bralower, 2002). Recent observations from ODP Site 756 (Viganò et al., 2023a) indicate a cold-eutrophic affinity of *Clausicoccus subdistichus* gr. (i.e., *C. subdistichus* and *C. fenestratus*).

The calcareous nannofossil diversity was estimated across the study interval using multiple diversity indices, since the application of one single index likely oversimplifies the real biodiversity signal. The indices adopted include the number of taxa (S), Dominance (D), Shannon-Weaver index (H) (Shannon & Weaver, 1949) and Evenness (E) (Buzas & Gibson, 1969). They are described in detail in the Supporting Information (Text S2). A significant relationship exists between diversity (indicated by the H index) and environmental stability. Low diversity and higher dominance (D) are often associated with more unstable, stressed, and eutrophic environments or during periods of disturbance (Wade & Bown, 2006; Wade & Pearson, 2008). In contrast, an assemblage with high evenness (E) has a relatively similar number of individuals in each species, suggesting ecological stability or constant/stable environmental conditions. For this purpose, multiple diversity indices were used as proxies to assess environmental stability and/or disturbance. Additionally, recognizing the possible connection between taxonomic diversity and preservation, we include calcium carbonate content (%) and additional information related to the nannofossil assemblages, such as the resistance or fragility of particular species and their relative abundances, to ensure the overall preservation quality throughout the entire interval.

2.4 Geochemical data

A total of 183 samples were powdered using an agate mortar and inserted into polyethylene capsules. For each sample, a mass of ~0.300 mg was weighed using a Mettler Toledo AT21 precision balance and placed into a borosilicate vial for analysis of bulk sediment carbon and oxygen stable isotope composition and calcium carbonate content (% $CaCO_3$). $CaCO_3$ content functions as a preservation indicator, helping to verify potential dissolution events along the studied interval. Simultaneously, $\delta^{13}C_{bulk}$ serves as a proxy for monitoring oceanic trophic changes and associated primary productivity as well as possible reservoir exchanges (e.g., Coxall & Wilson, 2011; Tagliabue & Bopp, 2008).

$\delta^{18}O_{bulk}$ primarily evaluates mixed-layer ocean conditions in term of temperature and glacial extension (Reghellin et al., 2019), and secondarily establishes correlations between these inferred conditions and observed changes in the calcareous nannofossil assemblages of the studied site. The oxygen isotopes measured in the bulk are also utilized to compare conditions in the mixed layer with those at the bottom, represented by the $\delta^{18}O$ benthic signature. Ultimately, $\delta^{18}O$ bulk data provides a valuable tool for correlation and evaluation of the completeness of the studied section based on the globally recognized stepwise pattern of oxygen isotopes, proving essential for site-to-site correlations (Viganò et al., 2023a).

The geochemical analysis was carried out at the University of Padova (Department of Geosciences) using a Delta V Advance Isotopic Ratio Mass Spectrometer equipped with a Gas Bench II device. Each sample was flushed with He5.5 and then treated with 10 drops of orthophosphoric acid (EMSURE ® ≥ 99%) for ca. 3 hours at 70°C. Isotopic values are reported in standard delta notation relative to the Vienna Pee Dee Belemnite (VPDB). For the calibration and the quality check, we used, respectively, two internal standards: Maq1 (white Carrara marble; $\delta^{13}C$= 2.58‰; $\delta^{18}O$= −1.15‰ VPDB) and Gr1 (marble; $\delta^{13}C$= 0.68‰; $\delta^{18}O$= −10.44‰ VPDB). On average, each run sequence comprised 45 samples, in addition to 12 Maq1 samples and 3 Gr1 samples, each one with a weight range between 0.200-0.250 mg. The precision of standards was better than 0.06‰ for $\delta^{13}C$ and better than 0.09‰ for $\delta^{18}O$, across all sample runs. Every run also contained a ramp of 8 samples of Maq1 with weights ranges from 0.050 to 0.500 mg equally distributed along the run. The Maq1 ramp samples allow the construction of a linear regression equation (based on the of CO_2 beam intensity - mV- and the standard weight - mg) to extrapolate $CaCO_3$ content of the investigated samples (Spofforth et al., 2010).

3 Results

3.1 Calcareous nannofossil assemblage records

Late Eocene to early Oligocene calcareous nannofossil assemblages at Site U1509 contain four main taxa, *Reticulofenestra, Coccolithus, Dictyococcites* and *Cyclicargolithus. Reticulofenestra* is the dominant component, with a mean abundance of ~67% across the ~5 Myr interval (Figure 2). *Reticulofenestra* specimens were subdivided into size groups (<4 µm, between 4-10 µm and 10-14 µm) to capture possible differences in the abundance behavior of these subgroups (Figure 3), as changes in coccolith size, observed both in recent and fossil taxa, can be linked to environmental variations (e.g. sea-surface temperatures, pCO_2, light availability or trophic load) (Finkel et al., 2010; Henderiks & Pagani, 2008; Ma et al., 2023). Additionally, coccolith-size shifts have been actively driven by selective pressures associated with Cenozoic climate

variations (Herrmann & Thierstein, 2012). The taxonomy of *Reticulofenestra* is typically intricate and ambiguous, leading to the frequent use of size groups (e.g., Toffanin et al., 2011). The use of these groups in paleoecology is also motivated by the fact that small reticulofenestrids are considered to be better adapted to eutrophic conditions. In modern oceans, small-size reticulofenestrids tend to thrive in regions characterized by high productivity (e.g. Hagino & Okada, 2001; Winter et al., 1994).

At Site U1509, the small, medium and large forms of *Reticulofenestra* have mean abundance values of ~26%, ~35% and 0.65% within the total assemblage. The larger forms (10-14 µm) record a slight decrease in abundance towards the top of the interval, medium-size forms (4-10 µm) have constant values throughout the interval, whereas smaller forms (<4 µm) increase in abundance towards the top (Figure 3).

Other relatively abundant calcareous nannofossils show trends over the EOT interval. *Coccolithus* represents the second most abundant taxon with a mean value across the study interval of 11.4% (Figure 2). Again, its abundance pattern varies, with a maximum peak of 20.7% in the upper part, although average values of ~13% are recorded between 267.30 and 240.90 m. *Dictyococcites* is a common component of the assemblages (on average ~8%; Figure 2). As for the reticulofenestrids, three groups have been differentiated based on their size (<4 µm, between 4-10 µm and 10-14 µm), and some specific taxa are also separated out (*D. bisectus* >10 µm, *D.* cf. *bisectus* <10 µm, *D. filewiczii* and *D. hesslandii*). These taxa are characterized by highly variable abundance through the study section (Figure 3), although the higher abundances are those of *D.* cf. *D. bisectus* (<10 µm) and *D. bisectus* (>10 µm), with mean values of 4.2% and 1.8%, respectively. All these taxonomic entities have been differentiated due to the distinct behavior documented in the literature (e.g. Bown & Dunkley Jones, 2012; Wei & Wise, 1990). *Cyclicargolithus* shows a distinct up-core abundance increase from ~2% in the lower part of the sections (below 217.36 m) to 8.4% in the overlying part of the section (Figure 2). Other key components in the assemblage, although with lower overall relative abundances, are detailed below. *Clausicoccus* (i.e., *C. subdistichus* and *C. fenestratus*) rapidly increases in abundance (from 7.1% to 11.5%) at 250.35 m with high values (~6.3% on average) that persisted up to 221.41 m and then rapidly dropped to a mean value of 0.1%. *Ericsonia* is rare at the base of the section, from 267.30 to 247.49 m, with a mean value of 1.4%. Above 247.49 m, *Ericsonia* displays a scattered decrease in abundance. Similarly, to *Ericsonia*, *Isthmolithus* is continuously present at the base of the interval with percentages <1.7%. *Discoaster* is rare to frequent in the lower part of the study interval with a peak in abundance (5.5%) between 267.30 and 256.96 m. *Discoaster* progressively decreases stratigraphically upward to values <1.2%. *Cribrocentrum* displays a similar pattern with a positive peak of 2.3% at 265.485 m and then gradually disappears. *Lanternithus* is a minor component of the lower Oligocene assemblage but displays a significant positive peak in abundance (up to 5.3%) at 242.70 m near the base of Chron C13n. Other components of the assemblage include *Blackites* (mean value 1.6%), *Sphenolithus* (mean value 1.5%), *Zygrhablithus* (mean value 1.1%), *Chiasmolithus* (mean value 0.4%), and *Helicosphaera* (mean value 0.1%). The category 'Others' includes very rare and discontinuous taxa, e.g., *Bramletteius, Coronocyclus, Markalius, Pontosphaera, Thoracosphaera, Umbilicosphaera* and indeterminate placoliths.

For the studied interval, at Site U1509, a low percentage (<1%) of the assemblage consists of middle-late Eocene reworked calcareous nannofossils (Figure 2). Examples of these are *Chiasmolithus consuetus, C.*

379 *eoaltus, C. expansus, C. grandis, C. solitus, Cribrocentrum isabellae, Discoaster lodoensis, D. multiradiatus,*
380 *D. praebifax, D. kuepperi, Neococcolithus dubius*. Reworked specimens are mainly recorded in the upper part
381 of the section, from 223.20 m to 183.30 m. The Supporting Information (Plates S1-S6) contains a compilation
382 of LM microphotos displaying selected calcareous nannofossil taxa including reworked specimens. These
383 images enable the identification of specific morphological features and the assessment of the preservation state
384 of calcareous nannofossils.
385
386 **3.2 Principal component analysis and diversity index**
387 The cumulative variation captured by the principal components likely represents the majority of the
388 variation of the original variables, assumed here to represent various environmental parameters. Therefore,
389 PCA serves as a valuable tool for simplifying complex data, offering an approach not directly obtainable
390 through time-series data or assemblage plots.
391 The PCA analysis (Q-mode) performed on the entire assemblage record provided two principal
392 components, PC1 and PC2. PC1 is characterized by a high negative loading on *Reticulofenestra* (-0.36) and
393 *Cyclicargolithus* (-0.30), whereas it is positively loaded on *Coccolithus* (0.37) and *Ericsonia* (0.35). PC2 is
394 loaded by *Clausicoccus* (0.51), *Lanternithus* (0.42) and *Zygrhablithus* (0.41). *Discoaster* and *Ericsonia* are
395 also significant (-0.22). PC1 scores gradually decrease up section, marked by a major shift at 257.10 m (Figure
396 6). PC2 includes two gradual shifts toward more positive values at 257.10 m and at 250.50 m respectively. At
397 240.90 m, PC2 starts to decrease.
398 The two main variance factors in the Q-mode PCA analysis conducted on placoliths, PC1 and PC2, account
399 for 24.3% and 11.6% respectively. PC1 is characterized by high negative loading on *Reticulofenestra* <4 μm
400 (-0.36), *Dictyococcites* 4-10 μm (-0.31) and *Cyclicargolithus floridanus* (-0.28), whereas high positive
401 loadings are found for *E. formosa* (0.36) and *C. pelagicus* (0.28). PC2 is high positively loaded by
402 *Clausicoccus* (0.51) and *Chiasmolithus* (0.43) and high negatively loaded by *Dictyococcites hesslandii* (-0.43)
403 (Figure 7).
404 The Shannon H index and the number of taxa (S) show an overall decrease across the investigated section,
405 from 2.32 to 1.20 and from 30 to 12, respectively. Dominance (D) and Evenness (e^H/S) have a mean value of
406 0.24 and 0.33 and display a marked shift at 257.10 m and at 250.50 m, respectively (Figure 6).
407
408 **3.3 Relative changes in the calcareous nannofossil assemblage**
409 Changes and trends in the calcareous nannofossil data allowed us to identify four intervals and 2
410 subintervals (1-4, Figure 4) across the ~5 Myr study record:
411 1) **Interval 1** (267.30 – 257.10 m)
412 2) **Interval 2** (256.81 – 250.50 m)
413 3) **Interval 3** (250.19 – 221.41 m), further subdivided into two sub-intervals:
414 • **Interval 3A** (250.19 – 240.90 m)
415 • **Interval 3B** (240.59 – 221.41 m)
416 4) **Interval 4** (213.60 – 183.30 m).

Distinguishing features of the four intervals are as follows.

Interval 1. Interval 1 is defined by relatively abundant rosette-shaped *Discoaster* and low abundances of *Clausicoccus* (0-3.5%). From the base to close to the top of this interval, *Discoaster* varies in abundance from 1.4 to 5.5%. At 257.10 m, discoasters abruptly decrease, with values never exceeding 1.2% for the rest of the succession. Common components of Interval 1 also include *D. filewiczii* and *D. hesslandii.* Secondary components of this interval are *Cribrocentrum* (0-2.3%) and *Ericsonia* (0-4.8%).

Interval 2. Interval 2 displays a sharp decline of discoasters (at 257.10 m) that abruptly decrease with values never exceeding 1.2% for the rest of the succession, and a first slight increase of *Clausicoccus subdistichus* gr. During this interval, the assemblage of Interval 1 is gradually replaced by cold water meso/eutrophic taxa, as documented by the remarkable increase of *R. daviesii* from ~3 to 12%.

Interval 3A. Subinterval 3A is characterized by the sudden increase of *Clausicoccus subdistichus* gr. starting from 33.95 Ma (Bc; Viganò et al., 2024a). The average abundance of this taxon is 2.8% but positive peaks in abundance (up to 13%) are observed in this subinterval. *Lanternithus minutus* shows positive peaks (up to 4.3%) during this subinterval.

Interval 3B. Subinterval 3B is characterized by a gradual decline of *Clausicoccus subdistichus* gr., *Lanternithus* and *R. daviesii*. *Coccolithus* also displays a remarkable decrease, returning to pre-interval values at the onset of Interval 4.

Interval 4. Interval 4 is denoted by the virtual absence of *Clausicoccus subdistichus* gr. and a significant increase in the abundance of *Cyclicargolithus.* The Oligocene assemblages consist of few dominant taxa with high numbers of individuals (i.e., *Reticulofenestra* and *Cyclicargolithus*).

3.4 Bulk sediment geochemical data

3.4.1 Carbonate content

Interval 1 (267.30 – 257.10 m) is characterized by the lowest $CaCO_3$ content of the entire succession, varying between 53% and 84% and averaging 71%. Interval 2 (256.81 – 250.50 m) is characterized by the highest values, ranging between ca. 70% and 100%. Above this interval, in the uppermost ~3.4 Myr (Intervals 3 and 4; i.e. from 250.19 to 183.30 m), the carbonate content has a mean value of 78.3% (± 6.8%). Therefore, the carbonate content increased during Interval 2 but not during the EOGM, in contrast to the findings of other sites, specifically in the Indian (ODP Site 756; Viganò et al., 2023a) and in the Pacific Ocean (Coxall et al., 2005; Coxall & Wilson, 2011).

3.4.2 Carbon stable isotopes

Bulk carbon stable isotope values range between 1.45‰ and 2.64‰ with an average value of 2.04‰ (± 0.24‰ σ) (Figure 5). In the lower part of the section (Interval 1; 267.30 – 257.10 m), $\delta^{13}C$ values have an average value of 2.21‰ (± 0.15‰). The following Interval 2 (256.81 – 250.50 m) is characterized by slightly lower mean values (2.15‰ ± 0.11‰). From 250.19 – 221.41 m (Interval 3), the $\delta^{13}C$ curve displays a trend to lower values with an average of 2.10‰ (± 0.23‰). In the lower part of Interval 3 (Subinterval 3A; 250.19 – 240.90 m) several positive peaks reaching values up to 2.64‰ occur just above the base of Chron C13n. From

213.60 to 183.30 m (Interval 4), $\delta^{13}C$ values are relatively low and stable with a range of 1.45 to 2.46 and an average of 1.82‰ (± 0.18‰).

3.4.3 Oxygen stable isotopes

Bulk oxygen stable isotope values vary between -0.11‰ and 0.78‰ across the studied interval, with a mean value of 0.41‰ ± 0.21‰ (σ). Interval 1 (267.30 – 257.10 m) is characterized by the lowest $\delta^{18}O$ mean values (0.10‰ ± ‰ 0.10). Oxygen isotope values sharply increase by ~0.4‰ between ~256.5 and ~257.4 m, marking the base of Interval 2 (256.81 – 250.50 m) (Figure 5). This shift is interpreted to correlate with the so-called "Late Eocene Event" (LEE) recorded at Sites 522 and 1218 (Katz et al., 2008), which may represent a failed glaciation or a transient cooling event (Hutchinson et al., 2021). The onset of this event is coincident with the extinction of *D. saipanensis* as recorded at Site U1509 (34.50 Ma; Viganò et al., 2024a) and is in perfect agreement with the data from Site 1218 (Coxall et al., 2005). The first step of increase in $\delta^{18}O$ values (Step 1) was not clearly identified at Site U1509. Presumably, it lies in a recovery gap between cores 29R and 28R (Figure 5). At the base of Interval 3 (250.19 – 221.41 m), a major positive $\delta^{18}O$ shift begins (EOIS) at 248.40 m (~33.8 Ma), roughly coincident with the increase in abundance of *C. subdistichus* gr., for which the Bc is 33.95 Ma (Viganò et al., 2024a). The base of EOIS has a $\delta^{18}O$ value of 0.28‰ while the top of this shift (33.66 ± 0.04 Ma; Viganò et al., 2024a) has a maximum $\delta^{18}O$ value of 0.72‰. EOIS thus represents a rapid $\delta^{18}O$ increase (0.44‰) within the lowermost part of Chron C13n. The highest values of $\delta^{18}O$ are recorded within Chron C13n, which roughly correlates with the global phase of maximum positive $\delta^{18}O$ values (EOGM) (Hutchinson et al., 2021). Throughout Interval 4 (213.60 – 183.30 m), $\delta^{18}O$ values display an average value of 0.45‰ (± 0.10‰).

4 Discussion

4.1 Paleoclimatic evolution

At Site U1509, calcareous nannofossil assemblages reveal several shifts in the relative abundance and diversity indices across the Eocene-Oligocene, suggesting a link between paleoclimate changes and the response of the local phytoplanktonic community. The paleoclimatic interpretation inferred from diversity indices and the PCA analysis received additional support by the relatively high $CaCO_3$ wt% (Figure 5), which indicates that no significant dissolution occurred throughout the study interval. Dissolution can indeed impact the composition of coccolith assemblages (Roth, 1994), resulting in diminished diversity values and potentially misleading environmental interpretations (Viganò et al., 2023b). Thus, principal components (PC1 and PC2 scores) are interpreted to reflect changes in sea surface temperature and paleoproductivity, respectively, based on the ecological preferences recorded for the primary loading taxa.

Notably, a significant change in the assemblage correlates with the base of Chron C13n, which in turn roughly corresponds to the onset of the EOGM (max $\delta^{18}O_{bulk}$ values). Specifically, the decrease in warm-water oligotrophic taxa (i.e., *D. barbadiensis*, *D. saipanensis* and *E. formosa*) is consistent with both enhanced eutrophic conditions and decreased temperatures, with the assemblage shifts primarily controlled by temperature and nutrients (Figure 6). The shift towards cooler and eutrophic assemblages appears to be a

consistent feature of the EOT (Viganò et al., 2023a), since published records from both low-middle and high latitudes suggest increased nutrient availability and cooler conditions (Bordiga et al., 2015; Diester-Haass, 1995; Diester-Haass, Robert, & Chamley, 1998; Diester-Haass & Zahn, 1996, 2001; Dunkley Jones, 2008; Fioroni et al., 2015; Jones et al., 2019; Persico & Villa, 2004; Villa et al., 2008, 2014, 2021). Based on trends and shifts in the diversity indices, PCA scores, and paleoecological groups, we subdivided the study interval into four phases: (1) late Eocene warm-oligotrophic phase, (2) precursor diversity-decrease phase, (3) early Oligocene cold-eutrophic phase and (4) steady-state cosmopolitan phase.

Late Eocene Warm-Oligotrophic Phase (35.29 to 34.50 Ma)

This phase is constrained to the lower part of the section (267.30 – 257.10 m) and is dominated by warm-water and oligotrophic taxa and by highly even and diverse assemblages. Positive peaks in warm-water taxa suggest sustained late Eocene warmer and oligotrophic conditions and/or a pre-glaciated world. Species richness recorded at Site U1509 is relatively high during this phase reaching 30 taxa, and changes significantly up-section. The high values observed in the Shannon index values during this phase indicate a highly diverse community structure. At the same time PC2 displays relatively low values, ranging from a minimum of -2.61 to a maximum of 0.46, likely reflecting a stable-warm and oligotrophic environment (Bown et al., 2004). The presence of a highly diversified community, mainly characterized by warm-oligotrophic taxa, is consistent with relatively low $\delta^{18}O$ values documented in the interval. The end of this phase is marked by the onset of the Late Eocene Event (LEE), which is coincident with the extinction of the warm-water *D. saipanensis* (34.50 Ma; Viganò et al., 2024a) and denotes the base of the EOT. The extinction of the last representative of the rosette-shaped discoasters can be interpreted as the first biotic response to cooling during the LEE (Dunkley Jones et al., 2008; Hutchinson et al., 2021; Pearson et al., 2008) (Figure 6).

Precursor Diversity-Decrease Phase (34.50 to 33.95 Ma)

During this interval (256.81 – 250.50 m), the marked decrease in warm-oligotrophic taxa suggests either extreme sensitivity of calcareous nannoplankton to minor perturbations in the thermo/nutricline, or a climate threshold that was able to trigger dramatic upheavals in the nannoplankton community. The marked decline of warm-oligotrophic taxa is likely related to a global transition towards cooler and higher nutrient conditions. During the precursor diversity-decrease phase, nannoplankton rapidly reacted to the cooler and eutrophic conditions displaying a contraction of the k-selected community and the expansion of select r-mode opportunist taxa (MacArthur & Wilson, 1967; Pianka, 1970). Major changes in calcareous nannofossil assemblages are also recorded by diversity indices, especially emphasized by the dramatic decrease in species richness (number of taxa) and Shannon indices. The shift from the Eocene warm-oligotrophic community to the Oligocene cold-eutrophic community occurred in a time window of ~550 kyr, suggesting a strong and prompt response of the nannofossil assemblage to oceanographic changes.

Early Oligocene Cold-Eutrophic Phase (33.95 to 32.24 Ma)

In the lower part of this interval (250.19 – 240.90 m), PC1 and warm-oligotrophs significantly decrease and PC2 progressively increases. This phase indicates a period of intense perturbation within the marine ecosystem. At Site U1509, the acme intervals of *Clausicoccus subdistichus* gr. and *Lanternithus* represent a distinct feature of the EOT that is considered to be related to a better adaptation of these taxa to the enhanced eutrophication hypothesized for the EOGM. These acme intervals are temporary events lasting for ~1.78 and 1.17 Myr, respectively, and the specific ecological affinities of *Clausicoccus subdistichus* gr. and *Lanternithus* allow these taxa to rapidly adapt to the new environmental conditions, becoming a fundamental component of earliest Oligocene assemblages. During this phase, Shannon index values gradually return to pre-transitional values, reaching new relatively stable values.

The early Oligocene cold-eutrophic phase, initiated in the uppermost part of Chron C13r (~33.95 Ma), is interpreted to reflect deep changes in ocean circulation which led to an intensified nutrient availability in surface waters, providing competitive advantage for cold eutrophic taxa. Positive peaks in cold eutrophic taxa, such as *Chiasmolithus* and *R. daviesii*, are recorded within Chron C13n, which corresponds to extreme glacial conditions (EOGM), suggesting a strong connection between climate and nannoplankton changes.

Steady-State Cosmopolitan Phase (32.24 to 30.57 Ma)

The steady-state cosmopolitan phase (213.60 – 183.30 m) is characterized by the persistent dominance of taxa belonging to the cosmopolitan/survivor-opportunist group, such as *Reticulofenestra* and *Cyclicargolithus*. Decreasing Shannon index values confirm discrete changes in the assemblage structure, as reported also by the gradual decrease in the number of taxa. The virtually constant diversity values (H) documented during this phase possibly reflect a more stable ocean configuration, suggesting a gradual shift to a 'new' adjusted state with different stable assemblages.

4.2 Comparative nannofossil analysis across high and mid-low latitudes

Within any given region, the nature of the water masses and their relationship with calcareous nannoplankton distribution and abundance, depends mainly on three closely interconnected factors: 1) the paleolatitude of the region 2) the degree of isolation, and 3) the types of currents. The relationship between paleolatitude and calcareous nannofossil distribution was meticulously documented by Wei and Wise (1990), who demonstrated the establishment of pronounced latitudinal gradients by the middle Eocene in the South Atlantic. A latitudinal thermal gradient was also previously identified by Kennett (1978) in the Southern Ocean, where he recognized distinct plankton biogeographic provinces during the Cenozoic.

In the following sections, we aim to interpret our findings in light of the key outcomes derived from studies conducted at high and mid-low latitudes on calcareous nannofossil assemblages.

High-latitude Insights: At Site 748 (Kerguelen Plateau), Villa et al. (2008) highlighted a notable shift in the Temperate-warm-water taxa (Twwt) index indicating a sudden and significant cooling event concurrent with the rapid $\delta^{18}O$ positive shift (here termed EOIS). This cooling event is followed by a general indication of cool surface-waters throughout the Oligocene based on nannofossil assemblages.

In a more recent investigation covering the Atlantic (Maud Rise) and Indian (Kerguelen Plateau) sectors of the Southern Ocean (paleolatitudes of ~65°-60°S), Villa et al. (2014) presented additional evidence supporting a gradual cooling trend. A more intense cooling was deduced through the identification of the establishment of a 'cool-water assemblage' at the base of Chron C13n. Interestingly, the authors noted the onset of a significant Southern Ocean eutrophication as early as 36.23 Ma (GTS20) (lower Chron C16n.2n), persisting throughout the Oligocene.

A noteworthy observation is that the eutrophication of the Southern Ocean began 1.7 million years earlier than at Site U1509. This temporal discrepancy suggests a nuanced and gradual pattern of eutrophication unfolding across different latitudes. The observed delay implies that the Southern Ocean experienced an earlier phase of enhanced nutrient availability and increased biological productivity compared to Site U1509. Such temporal variations in eutrophication initiation may be linked to diverse environmental dynamics and oceanographic conditions prevailing at high and middle latitudes. Factors such as local climate, ocean circulation patterns, and proximity to nutrient sources could contribute to the observed temporal lag of eutrophication. Further investigations into the specific mechanisms driving these variations will provide valuable insights into the complex interplay between environmental factors and biological responses across different latitudinal zones.

Regional Insights: In the late Eocene, the central Tasman Sea, as evidenced by DSDP Site 283, displayed indications of warm surface waters characterized by the presence of rare discoasters and high diversity of calcareous nannofossils (Edwards & Perch-Nielsen, 1975). Conversely, ODP Site 1172, situated in the eastern Tasmanian margin, exhibited a scarcity of late Eocene discoasters and a low diversity of calcareous nannofossils, implying cooler water conditions (Exon, Kennett, Malone et al., 2001). These contrasting findings suggest a surface-temperature gradient between the two sites during the late Eocene. It is likely that warm-subtropical currents flowing southward were dominant at Site 283, while they failed to reach Site 1172, leading to cooler water conditions (Kennett & Exon, 2004).

It is crucial to recognize that most previous nannofossil records from the Southwestern Pacific, including data from Site 592 (southern Lowe Howe Rise; Kennett et al., 1982), are primarily qualitative and often focused on shipboard biostratigraphic data. Consequently, past paleoenvironmental inferences at these sites rely on the presence or absence of taxa, particularly warmth-indicating taxa (e.g., discoasters) rather than quantitative distribution (%). At the Campbell Plateau (DSDP Site 277), paleotemperature reconstructions based on the *Discoaster*/*Chiasmolithus* ratio indicate a warming trend from the late middle Eocene onwards, followed by cooling in the latest Eocene (Waghorn, 1981; Kennett & Exon, 2004). The similarity of our data with previous qualitative records from the Southwestern Pacific suggests the presence, during the late Eocene, of a widespread warm subtropical proto-East Australian Current (pEAC) extending from the NCT to the central Tasman Sea with few exceptions (e.g. Site 1172). This trend aligns with the proposed tropical temperatures at middle-high latitudes during the middle and late Eocene (Liu et al., 2009; Bijl et al., 2010). Notably, reconstructions based on radiolarian assemblages at the same sites indicate the existence of cold-water taxa and endemic Antarctic taxa since the middle Eocene, but they distinguish the conditions observed at Site 283

(warmer) from those at Site 1172 (cooler) (Pascher, 2017; Pascher et al., 2015). The heightened sensitivity of radiolarians to temperature variations allows for the presence of cold taxa even with extremely limited temperature changes since the middle Eocene.

In summary, the paleotemperature reconstructions in the region align seamlessly with the nannofossil dataset, suggesting consistently mild temperatures in the middle to late Eocene, possibly due to the southward extension of the East Australian Current (EAC).

Mid-low latitude Insights: Bordiga et al. (2015) associated the progressive decline of the absolute abundances of nannofossils during the EOT at Site 1263 (Walvis Ridge, Atlantic Ocean), to the Southern Ocean cooling. Nannofossil data from Java (NKK1 borehole, equatorial Indo-Pacific) indicated a significant drop in diversity coinciding with the extinction of rosette-shaped discoasters and a shift from strongly oligotrophic to more mesotrophic conditions (Jones et al., 2019). A recent study from the Equatorial Indian Ocean (Site 709) suggested increased sea-surface nutrient availability (starting from the base of Chron C15n) possibly linked to the formation at high latitudes of nutrient-rich waters (Villa et al., 2021).

The major changes observed in the calcareous nannofossil assemblage at Site U1509, in terms of both timing and nature, closely resemble those recorded in the Indo-Pacific (Java; Jones et al., 2019), in the equatorial (ODP Site 711; Fioroni et al., 2015) and in the mid-latitude Indian Ocean (Site 756, Viganò et al., 2023a), indicating a basin-wide Indo-Pacific response. This connection between low and middle latitudes could be attributed to the establishment of a shallow marine connection between the southern Indian Ocean and the Pacific across the South Tasman Rise (e.g., the Tasmanian Gateway), that could have triggered the production of cold-eutrophic bottom waters near the beginning of the Oligocene (Stickley et al., 2004).

4.3 Major changes in calcareous nannofossil placoliths

The EOT represents a tipping point in the Cenozoic climate evolution, documenting the transition from warm-oligotrophic to cold-eutrophic communities, dominated by a few opportunistic taxa. Data collected at Site U1509 allow us to analyze the tempo and mode of this transition, as well as the biodiversity community structure. However, the role of placoliths, the dominant component of calcareous nannofossil assemblages, still remains undetermined. To resolve this, an additional PCA was performed on this component, which is distributed in different quadrants (i.e. time) in the PCA biplot (Figure 7).

In particular, *C. pelagicus, Cribrocentrum, D. hesslandii, D. filewiczii* and medium size (4-10 µm) reticulofenestrids, as well as the above-mentioned *E. formosa* are distributed in the right lower quadrant in the PCA plot suggesting an affinity for warm and oligotrophic conditions. Samples documenting the transitional (i.e. the *precursor diversity-decrease phase*) and EOGM conditions are instead distributed in the right upper quadrants and are characterized by the higher abundances of the following placoliths: *D. bisectus* gr., large-sized reticulofenestrids (10-14 µm and >14 µm), *Clausicoccus, Chiasmolithus* and *R. daviesii*.

Finally, the earliest Oligocene assemblages, distributed in the left upper quadrant are dominated by small reticulofenestrids (<4 µm), small to medium size *Dictyococcites*, and *C. floridanus*. This latter assemblage supports the hypothesis that, once the steady-state cosmopolitan phase was reached, the new environmental

conditions, characterized by cold and nutrient enriched waters, persisted for at least 1.8 Myrs. Further support for an early Oligocene eutrophication at Site U1509 is provided by the presence of small opportunist reticulofenestrids (<4 μm), as observed at ODP Site 756 (Viganò et al., 2023a).

4.4 Bulk and Benthic Stable Isotopes

To improve the comprehension and applicability of bulk carbonate stable isotopes in paleoenvironmental analysis, we have compared our bulk isotopic record from Site U1509 in the Southwestern Pacific with the benthic reference record from the eastern equatorial Pacific Site 1218 (Coxall & Pearson, 2007; Coxall & Wilson, 2011). Despite lower resolution through the sequence and the discontinuous recovery in the early Oligocene, the $\delta^{13}C_{bulk}$ and $\delta^{18}O_{bulk}$ records at Site U1509 mirror the more complete and highly resolved $\delta^{13}C_{benth}$ and $\delta^{18}O_{benth}$ profiles at Site 1218. The comparison of these two records highlights the well-known vertical gradient existing between surface and bottom waters (e.g. Boyle, 1988). As expected, the absolute values are heavier in the benthic records (e.g. $\delta^{18}O_{benth}$ 0–1.5‰) representing bottom water conditions, while the lighter bulk sediment isotopic signal ($\delta^{18}O_{bulk}$ 0-0.8‰) primarily reflects sea-surface conditions. These results likely provide further support to the idea that bulk stable carbon and oxygen isotopes derived from sediments containing abundant and well-preserved nannofossils may be used as a proxy for mixed layer conditions (Reghellin et al., 2015; 2019; Viganò et al., 2023b). Nevertheless, the importance of biological fractionation ("vital effects") of a single taxon still remains, and a global signature could be enhanced, attenuated, or completely blurred by the ecological and metabolic behavior of different taxa belonging to the same microfossil group. In addition, minor differences/issues can come from instrumental offsets when comparing absolute stable isotopic values, even with the use of standards intended to mitigate this effect. To fully grasp and address this offset, a comprehensive analysis necessitates the comparison of multiple bulk and benthic records, which unfortunately are seldom available in the existing literature. A preliminary observation indicates that the global benthic signal is discernible in the bulk record, suggesting a connection between the observed patterns in the two profiles and global processes. A significant aspect supporting this interpretation is that both the general trend and specific details such as minor cooling phases (e.g., LEE; Figure 5) can be recognized in the bulk isotopic signal, mirroring those present in the benthic isotope curve.

In the sub-Antarctic Deep Sea Drilling Project (DSDP) Site 277, with a paleodepth between 2200-2800 m, the C and O stable isotopes display the typical surface-to-deep gradient (Pascher et al., 2015) with benthic (*Cibicidoide*s spp.) records that significantly differ from the bulk and deep-dweller planktonic foraminifera (*Subbotina* spp.) records, which instead perfectly overlap. In addition, $\delta^{18}O$ bulk values across the EOT at Site 277 range from 0.44‰ to ~1‰ (Pascher et al., 2015), and are comparable, within instrumental error, to those of Site U1509 (~0.2‰-0.7‰).

It is noteworthy that calcareous nannoplankton taxa inhabiting high latitudes (e.g., Site 277; Pascher et al., 2015) demonstrate significant differences from those thriving at low-middle latitudes (e.g., Site U1509, this study; Site 756, Viganò et al., 2023a). However, discernible differences in the isotopic profiles are not apparent, implying that the vital effect is likely a minor contributor to the bulk isotope signature.

4.5 Paleoceanographic evolution in the Southwestern Pacific

The observed variations in biotic and geochemical proxies at Site U1509 indicate an initial change of the Southern Ocean circulation during the latest Eocene, coinciding with the onset of the EOT. In the following, we integrate our results into a broader context of regional to global climate specifically considering results from radiolarian studies in the region (Pascher, 2017), the recent discoveries related to surface water currents in the late Eocene (Sauermilch et al., 2021; Nooteboom et al., 2022) and the timing and duration of the eutrophication in the equatorial Pacific (Coxall et al., 2011).

The late Eocene decline in warm-oligotrophic water taxa at Site U1509 aligns with available data from the Tasman Sea, which generally indicates a late Eocene cooling. This cooling led to the northward expansion of the proto-Ross Gyre (pRG) to the Campbell Plateau (Site 277) (Pascher, 2017), and the presence of distinct latitudinal thermal gradients based on dinocyst associations (Bijl et al., 2018). Additionally, extensive non-deposition occurred in the central (Site 283), southwest (Sites 281 and 1172), and northern Tasman Sea (Sites 206 and 207), possibly indicating strengthened northward flowing bottom currents and/or tectonic processes related to subduction (Site 206 and 207, Sutherland et al., 2010). An exception was Site 592, approximately 200 km south of Site U1509, which, along with U1509, preserved a complete Eocene-Oligocene transition (EOT) sequence.

The observed early Oligocene enhanced eutrophication at Site U1509 may be linked to a crucial aspect of the late Eocene-early Oligocene paleoceanographic reorganization: the development of a proto-Antarctic Circumpolar Current (pACC) (e.g. Kennett et al., 1975a; Sarkar et al., 2019; Sauermilch et al., 2021; Scher et al., 2015). This evolution likely intensified nutrient transport by southern water masses, leading to heightened upwelling systems at middle-high latitudes (Kennett et al., 1975a). However, recent models highlight that even slight depth adjustments in ocean gateways significantly impact ocean circulation patterns and Antarctic surface waters (Sauermilch et al., 2021). According to these models, the openings primarily result in the weakening of oceanic gyres rather than the establishment of a robust pACC, which was notably weaker than it is today.

In conclusion, the eutrophication lasting ~700 kyrs observed at Site U1509 and corresponding to the earliest Oligocene Glacial Maximum (EOGM), strongly correlates with the enhanced productivity reported in the Eastern Equatorial Pacific at ODP Site 1218 (Coxall and Wilson, 2011), lasting approximately ~500 kyrs and associated with Chron C13n. This shared feature suggests a connection between low and middle latitudes, likely attributable to the expansion of deep mixing at high latitudes and the presence of common nutrient-rich waters.

Although not explicitly recognized, the decrease of warm and oligotrophic conditions, which are followed by a drop of calcareous nannofossil diversity and by the progressive increase of cold and eutrophic conditions, are indeed evident and documented in numerous available datasets, indicating a significant and coherent global evolution during the late Eocene to early Oligocene, as well as a strong teleconnection between low, middle, and high latitudes (Coxall & Wilson, 2011; Cramer et al., 2009; Dunkley Jones et al., 2008; Houben et al., 2013; Salamy & Zachos, 1999; Tibbett et al., 2021; Villa et al., 2021).

5 Conclusions

Nannofossil assemblage data from Site U1509 reveal a major shift from a late Eocene community characterized by warm and oligotrophic taxa, to an early Oligocene opportunistic assemblage, better adapted to colder and more eutrophic conditions. Our results suggest that this shift in the assemblage composition was driven by sea-surface water cooling and eutrophication caused by the inception of a proto-ACC, which resulted in the northward transport of cooler and nutrient-rich Antarctic waters. These mid-latitude changes highlight the impact of high latitude cryosphere changes on lower latitude ecosystems. The four paleoclimate intervals identified at Site U1509 reveal synchronous shifts in mid-latitude physical oceanography and marine phytoplankton communities. The most prominent turnover in the calcareous nannofossil assemblages took place during the *precursor diversity-decrease phase*, a transitional time interval of ~550 kyrs within the EOT.

In the Tasman Sea, the increase in marine productivity reached maximum values at the EOGM, as inferred from the high abundance of cold-eutrophic taxa and PC2 score, implying larger-scale effects on the nannoplankton community associated with sea ice formation and ocean overturning. However, nannofossil assemblage data indicate that increased nutrient availability and productivity may have persisted until at least ~32 Ma, although with reduced intensity. The Oligocene steady-state cosmopolitan phase is characterized by three dominant genera and by cold temperature and eutrophic conditions.

The role of the tectonic opening of the Southern Ocean gateways in the Antarctic glaciation is often considered neglected (DeConto & Pollard, 2003; Huber et al., 2004; Zhonghui et al., 2009); however our data highlights that evolving oceanographic conditions and invigorated oceanic circulation around Antarctica (Houben et al., 2019; Sauermilch et al., 2021), including deep and surface ocean cooling (Bohaty et al, 2012; Cramwinckel et al., 2018; Sauermilch et al., 2021; Sijp et al., 2011), undoubtedly influenced and shaped calcareous nannofossil assemblages during the EOT (e.g. Viganò et al., 2023a; Villa et al., 2021).

Acknowledgments

The authors thank: the International Ocean Discovery Program (IODP), for providing samples and data used in this study; all members of RV JOIDES Resolution IODP Expedition 371, for helping to collect and document samples; Isabella Raffi and Davide Persico, for their constructive comments in the capacity of reviewers of A.V.' s PhD thesis; Matthew Huber (Editor), the Associate Editor, and the reviewer, Peter Bijl, for their constructive feedback. Funding for A.V. and C.A. was provided by University of Padova and a RETURN Extended Partnership, financed by the National Recovery and Resilience Plan – NRRP, Mission 4, Component 2, Investment 1.3 – D.D. 1243 2/8/2022, PE0000005. E.D. was supported by the Deutsche Forschungsgemeinschaft (DFG, grants 408178503 and 465492305). L.A. received support from project PID2019-105537RB-I00 (Spanish Ministry of Science and Innovation and FEDER funds), funded by MCIN/AEI/10.13039/501100011033 and by "ERDF A way of making Europe.".

Open Research

Data presented in this study are archived at PANGAEA (https://doi.pangaea.de/) under the CC-BYCC0: Creative Commons Zero 1.0 Universal License. Calcareous nannofossil assemblage data (%) can be found in Viganò et al. (2024b). Bulk stable isotopes and carbonate content are available in Viganò et al. (2024c).

References

Agnini, C., Fornaciari, E., Raffi, I., Catanzariti, R., Pälike, H., Backman, J., & Rio, D. (2014). Biozonation and biochronology of Paleogene calcareous nannofossils from low and middle latitudes. *Newsletters on Stratigraphy*, *47*(2), 131–181. https://doi.org/10.1127/0078-0421/2014/0042

Agnini, C., Monechi, S., & Raffi, I. (2017). Calcareous nannofossil biostratigraphy: historical background and application in Cenozoic chronostratigraphy. *Lethaia*, *50*(3), 447–463. https://doi.org/10.1111/let.12218

Anagnostou, E., John, E. H., Edgar, K. M., Foster, G. L., Ridgwell, A., Inglis, G. N., … Pearson, P. N. (2016). Changing atmospheric CO_2 concentration was the primary driver of early Cenozoic climate. *Nature*, *533*, 380–384. https://doi.org/10.1038/nature17423

Aubry, M.-P. (1984). *Handbook of Cenozoic calcareous nannoplankton, book 1, Ortholithae (Discoaster)*. New York: American Museum of Natural History Micropaleontology Press.

Aubry, M.-P. (1988). *Handbook of Cenozoic calcareous nannoplankton, book 2, Ortholithae (Holococcoliths, Ceratoliths and others).* New York: American Museum of Natural History Micropaleontology Press.

Aubry, M.-P. (1989). *Handbook of Cenozoic Calcareous Nannoplankton, book 3, Ortholithae (Pentaliths, and Others) Heliolithae (Fasciculiths, Sphenoliths and Others)*. New York: American Museum of Natural History Micropaleontology Press.

Aubry, M.-P. (1992). Late Paleogene Calcareous Nannoplankton Evolution: A Tale of Climatic Deterioration. In *Eocene-Oligocene Climatic and Biotic Evolution* (pp. 272–279). https://doi.org/10.1515/9781400862924.272

Aubry, M.-P. (1998). Early Paleogene Calcareous nannoplankton evolution: a tale of climatic amelioration. In M.-P. Aubry & et al. (Eds.), *Late Paleocene–early Eocene Biotic and Climatic Events in the Marine and Terrestrial Records* (pp. 158–201). New York: Columbia University Press.

Backman, J. (1980). Miocene-Pliocene nannofossils sedimentation rates in the Hatton-Rockall basin, NE Atlantic Ocean. Acta Univ. *Stockholm Contributions in Geology*, *36*, 1–93. Retrieved from https://ci.nii.ac.jp/naid/10003977010/

Bijl, P. K., Houben, A. J. P., Hartman, J. D., Pross, J., Salabarnada, A., Escutia, C., & Sangiorgi, F. (2018). Paleoceanography and ice sheet variability offshore Wilkes Land, Antarctica - Part 2: Insights from Oligocene-Miocene dinoflagellate cyst assemblages. *Climate of the Past*, *14*(7), 1015–1033. https://doi.org/10.5194/cp-14-1015-2018

Bohaty, S. M., Zachos, J. C., & Delaney, M. L. (2012). Foraminiferal Mg/Ca evidence for Southern Ocean cooling across the Eocene-Oligocene transition. *Earth and Planetary Science Letters*, *317–318*, 251–261. https://doi.org/10.1016/j.epsl.2011.11.037

Bordiga, M., Henderiks, J., Tori, F., Monechi, S., Fenero, R., Legarda-Lisarri, A., & Thomas, E. (2015).

Microfossil evidence for trophic changes during the Eocene-Oligocene transition in the South Atlantic (ODP Site 1263, Walvis Ridge). *Climate of the Past*, *11*, 1249–1270. https://doi.org/10.5194/cp-11-1249-2015

Bordiga, M., Sulas, C., & Henderiks, J. (2017). Reticulofenestra daviesii: biostratigraphy and paleogeographic distribution across the Eocene–Oligocene boundary. *Geobios*, *50*(5–6), 349–358. https://doi.org/10.1016/j.geobios.2017.07.002

Bostock, H. C., Hayward, B. W., Neil, H. L., Sabaa, A. T., & Scott, G. H. (2015). Changes in the position of the Subtropical Front south of New Zealand since the last glacial period. *Paleoceanography*, *30*, 824–844. https://doi.org/10.1002/2014PA002652.Received

Bostock, H. C., Sutton, P. J., Williams, M. J. M., & Opdyke, B. N. (2013). Reviewing the circulation and mixing of Antarctic Intermediate Water in the South Pacific using evidence from geochemical tracers and Argo float trajectories. *Deep-Sea Research Part I: Oceanographic Research Papers*, *73*, 84–98. https://doi.org/10.1016/j.dsr.2012.11.007

Boyle, E. A. (1988). The role of vertical chemical fractionation in controlling late Quaternary atmospheric carbon dioxide. *Journal of Geophysical Research: Oceans*, *93*(C12), 15701–15714. https://doi.org/https://doi.org/10.1029/JC093iC12p15701

Bown, P. R. (1998). *Calcareous nannofossil biostratigraphy*. London, UK: Chapman and Hall (Kluwer Academic Publishers).

Bown, P. R. (2005). Paleogene calcareous nannofossils from the Kilwa and Lindi areas of coastal Tanzania (Tanzania Drilling Project 2003-4). *Journal of Nannoplankton Research*, *27*(1), 21–95.

Bown, P. R., & Dunkley Jones, T. (2012). Calcareous nannofossils from the Paleogene equatorial Pacific (IODP Expedition 320 Sites U1331-1334). *Journal of Nannoplankton Research*, *32*(2), 3–51.

Bown, P. R., Lees, J. A., & Young, J. R. (2004). *Calcareous nannoplankton evolution and diversity through time*. (H. R. Thierstein & J. R. Young, Eds.), *Coccolithophores - From Molecular Process to Global Impact*. London: Springer. https://doi.org/10.1007/978-3-662-06278-4_18

Bown, P. R., & Young, J. R. (1998). Techniques. In P.R. Bown (Ed.), *Calcareous nannofossil biostratigraphy* (pp. 16–28). London: Kluwer Academic Publishers.

Bralower, T. J. (2002). Evidence of surface water oligotrophy during the Paleocene-Eocene Thermal Maximum: nannofossil assemblage data from Ocean Drilling Program Site 690, Maud Rise, Weddell Sea. *Paleoceanography*, *17*(2), 1023. https://doi.org/10.1029/2002PA000832

Bukry, D. (1973). Low-latitude coccolith biostratigraphic zonation. *Initial Reports of the Deep Sea Drilling Project*, *15*, 685–703. https://doi.org/10.2973/dsdp.proc.15.116.1973

Buzas, M. A., & Gibson, T. G. (1969). Species diversity: benthonic foraminifera in Western North Atlantic. *Science*, *163*(3862), 72–75. https://doi.org/10.1126/science.163.3862.72

Cande, S. C., & Stock, J. M. (2004). Pacific-Antarctic-Australia motion and the formation of the Macquarie Plate. *Geophysical Journal International*, *157*(1), 399–414. https://doi.org/10.1111/j.1365-246X.2004.02224.x

Carter, L., Carter, R. M., & McCave, I. N. (2004). Evolution of the sedimentary system beneath the deep

Pacific inflow off eastern New Zealand. Marine Geology, 205(1–4), 9–27. https://doi.org/10.1016/S0025-3227(04)00016-7

Carter, R. M. (1985). The mid-Oligocene Marshall Paraconformity, New Zealand: coincidence with global eustatic sea-level fall or rise? The Journal of Geology, 93(3), 359–371. https://doi.org/10.1086/628957

Carter, R. M., & Landis, C. A. (1972). Correlative Oligocene Unconformities in Southern Australasia. Nature Physical Science, 237(70), 12–13. https://doi.org/https://doi.org/10.1038/physci237012a0

Chiswell, S. M., Bostock, H. C., Sutton, P. J. H., & Williams, M. J. (2015). Physical oceanography of the deep seas around New Zealand: A review. *New Zealand Journal of Marine and Freshwater Research*, *49*(2), 286–317. https://doi.org/10.1080/00288330.2014.992918

Chiswell, S. M., Toole, J., & Church, J. (1997). Transports across the Tasman Sea from WOCE repeat sections: The East Australian Current 1990–94. *New Zealand Journal of Marine and Freshwater Research*, *31*, 469–475. https://doi.org/10.1080/00288330.1997.9516780

Close, D. I., Watts, A. B., & Stagg, H. M. J. (2009). A marine geophysical study of the Wilkes Land rifted continental margin, Antarctica. Geophysical Journal International, 177(2), 430–450. https://doi.org/10.1111/j.1365-246X.2008.04066.x

Coxall, H. K., & Pearson, P. N. (2007). The Eocene-Oligocene Transition. In M. Williams, A. M. Haywood, J. Gregory, & D. N. Schmidt (Eds.), *Deep-Time Perspectives on Climate Change: Marrying the Signal from Computer Models and Biological Proxies, Micropaleontology Society Special Publication* (pp. 351–387). London: Geological Society.

Coxall, H. K., & Wilson, P. A. (2011). Early Oligocene glaciation and productivity in the eastern equatorial Pacific: Insights into global carbon cycling. *Paleoceanography*, *26*(2), 1–18. https://doi.org/10.1029/2010PA002021

Coxall, H. K., Wilson, P. A., Pälike, H., Lear, C. H., & Backman, J. (2005). Rapid stepwise onset of Antarctic glaciation and deeper calcite compensation in the Pacific Ocean. *Nature*, *433*(7021), 53–57. https://doi.org/10.1038/nature03135

Cramer, B. S., Toggweiler, J. R., Wright, J. D., Katz, M. E., & Miller, K. G. (2009). Ocean overturning since the Late Cretaceous: Inferences from a new benthic foraminiferal isotope compilation. *Paleoceanography*, *24*, PA4216. https://doi.org/10.1029/2008PA001683

Cramwinckel, M. J., Huber, M., Kocken, I. J., Agnini, C., Bijl, P. K., Bohaty, S. M., … Sluijs, A. (2018). Synchronous tropical and polar temperature evolution in the Eocene letter. *Nature*, *559*(7714), 382–386. https://doi.org/10.1038/s41586-018-0272-2

Dallanave, E., Maurizot, P., Agnini, C., Sutherland, R., Hollis, C. J., Collot, J., … Morgans, H. E. G. (2020). Eocene (46-44 Ma) onset of Australia-Pacific plate motion in the southwest Pacific inferred from stratigraphy in New Caledonia and New Zealand. *Geochemistry, Geophysics, Geosystems*, *21*(7). https://doi.org/10.1029/2019GC008699

Dallanave, E., Sutherland, R., Dickens, G. R., Chang, L., Tema, E., Alegret, L., … von Dobeneck, T. (2022). Absolute Paleolatitude of Northern Zealandia From the Middle Eocene to the Early Miocene. *Journal of Geophysical Research: Solid Earth*, *127*, e2022JB024736. https://doi.org/10.1029/2022jb024736

DeConto, R. M., & Pollard, D. (2003). Rapid Cenozoic glaciation of Antarctica induced by declining atmospheric CO_2. *Nature*, *1317*(2001), 1313–1317.

Diester-Haass, L. (1995). Middle Eocene to early Oligocene paleoceanography of the Antarctic Ocean (Maud Rise, ODP Leg 113, Site 689): change from a low to a high productivity ocean. *Palaeogeography, Palaeoclimatology, Palaeoecology*, *113*(2–4), 311–334. https://doi.org/10.1016/0031-0182(95)00067-V

Diester-Haass, L., Robert, C., & Chamley, H. (1998). Paleoproductivity and climate variations during sapropel deposition in the Eastern Mediterranean Sea. *Proceedings of the Ocean Drilling Program, Scientific Results*, *160*, 227–248.

Diester-Haass, L., & Zahn, R. (1996). Eocene-Oligocene transition in the Southern Ocean: History of water mass circulation and biological productivity. *Geology*, *24*(2), 163–166. https://doi.org/10.1130/0091-7613(1996)024<0163:EOTITS>2.3.CO;2

Diester-Haass, L., & Zahn, R. (2001). Paleoproductivity increase at the Eocene - Oligocene climatic transition: ODP/DSDP sites 763 and 592. *Palaeogeography, Palaeoclimatology, Palaeoecology*, *172*(1–2), 153–170. https://doi.org/10.1016/S0031-0182(01)00280-2

Dunkley Jones, T. (2008). *The response of low-latitude calcareous phytoplankton to global change through the Eocene-Oligocene transition*.

Dunkley Jones, T., Bown, P. R., Pearson, P. N., Wade, B. S., Coxall, H. K., & Lear, C. H. (2008). Major shifts in calcareous phytoplankton assemblages through the Eocene-Oligocene transition of Tanzania and their implications for low-latitude primary production. *Paleoceanography*, *23*(4), 1–14. https://doi.org/10.1029/2008PA001640

Edwards, A. R., & Perch-Nielsen, K. (1975). Calcareous Nannofossils from the Southern Southwest Pacific, Deep Sea Drilling Project, Leg 29,. In J. P. Kennett & R. E. Houtz (Eds.), *Initial Report of the Deep Sea Drilling Program* (pp. 469–539).

Etienne, S., Collot, J., Sutherland, R., Patriat, M., Bache, F., Rouillard, P., … Juan, C. (2018). Deepwater sedimentation and Cenozoic deformation in the Southern New Caledonia Trough (Northern Zealandia, SW Pacific). *Marine and Petroleum Geology*, *92*, 764–779. https://doi.org/10.1016/j.marpetgeo.2017.12.007

Exon, N. F., Kennett, J. P., Malone, M. J., Brinkhuis, H., Chaproniere, G. C. H., Ennyu, A., . . . Scroggs, J. M. (2001). Leg 189 Summary . Proceedings of the Ocean Drilling Program, Part A: Initial Reports, Vol. 189, 98p.. doi:10.2973/odp.proc.ir.189.101.2001

Exon, N., Kennett, J., Malone, M., Brinkhuis, H., Chaproniere, G., Ennyu, A., . . . White, T. (2000). *The opening of the Tasmanian Gateway drove global Cenozoic paleoclimatic and paleoceanographic changes; results of Leg 189* . Joint Oceanographic Institutions for Deep Earth Sampling, Palisades, NY, United States.

Falkowski, P. G., Katz, M. E., Knoll, A. H., Quigg, A., Raven, J. A., Schofield, O., & Taylor, F. J. R. (2004). The evolution of modern eukaryotic phytoplankton. Science, 305(5682), 354–360. https://doi.org/10.1126/science.1095964

907 Finkel, Z. V., Beardall, J., Flynn, K. J., Quigg, A., Rees, T. A. V., & Raven, J. A. (2010). Phytoplankton in a
908 changing world: Cell size and elemental stoichiometry. *Journal of Plankton Research*, *32*(1), 119–137.
909 https://doi.org/10.1093/plankt/fbp098
910 Fioroni, C., Villa, G., Persico, D., & Jovane, L. (2015). Middle Eocene-Lower Oligocene calcareous
911 nannofossil biostratigraphy and paleoceanographic implications from Site 711 (equatorial Indian
912 Ocean). *Marine Micropaleontology*, *118*, 50–62. https://doi.org/10.1016/j.marmicro.2015.06.001
913 Fulthorpe, C. S., Carter, R. M., Miller, K. G., & Wilson, J. (1996). Marshall Paraconformity: a mid-Oligocene
914 record of inception of the Antarctic circumpolar current and coeval glacio-eustatic lowstand? *Marine*
915 *and Petroleum Geology*, *13*(1), 61–77.
916 Gaina, C., Müller, R.D., Royer, J.Y., Stock, J., Hardebeck, J., Symonds, P. (1998). The tectonic history of the
917 Tasman Sea: A puzzle with 13 pieces. Journal of Geophysical Research 103, 12413–12433.
918 https://doi.org/10.1029/98JB00386
919 Gradstein, F. M., Ogg, J. G., Schmitz, M. D., & Ogg, G. M. (2020). *Geological Time Scale 2020*. Elsevier.
920 Hagino, K., & Okada, H. (2001). Morphological observations of living Gephyrocapsa crassipons. *Journal of*
921 *Nannoplankton Research*, *23*(1), 3–7.
922 Haiblen, A. M., Opdyke, B. N., Roberts, A. P., Heslop, D., & Wilson, P. A. (2019). Midlatitude Southern
923 Hemisphere Temperature Change at the End of the Eocene Greenhouse Shortly Before Dawn of the
924 Oligocene Icehouse. *Paleoceanography and Paleoclimatology*, *34*, 1995–2004.
925 https://doi.org/10.1029/2019PA003679
926 Hallock, P. (1987). Fluctuations in the trophic resource continuum: A factor in global diversity cycles?
927 *Paleoceanography*, *2*(5), 457–471.
928 Hamilton, L. J. (2006). Structure of the Subtropical Front in the Tasman Sea. *Deep-Sea Research*, *53*(12),
929 1989–2009. https://doi.org/10.1016/j.dsr.2006.08.013
930 Hammer, Ø., Harper, D. T., & Ryan, D. D. (2001). Past: Paleontological Statistics Software Package for
931 Education and Data Analysis. *Palaeontologia Electronica*, *4*(4), 5–7.
932 https://doi.org/10.1016/j.bcp.2008.05.025
933 Haq, B. U. (1971). Paleogene Calcareous Nannoflora: Part II. Oligocene of Western Germany. *Stockholm*
934 *Contributions in Geology*, *25*(2), 57–133.
935 Haq, B. U. (1973). Transgressions, climatic change and the diversity of calcareous nannoplankton. *Marine*
936 *Geology*, *15*(2), M25–M30.
937 Harper, D. A. T. (1999). Numerical Palaeobiology. Computer-Based Modelling and Analysis of Fossils and
938 their Distributions. In *Geological Magazine* (468 pp.). John Wiley & Sons.
939 https://doi.org/10.1017/s0016756800214416
940 Henderiks, J., & Pagani, M. (2008). Coccolithophore cell size and the Paleogene decline in atmospheric CO2.
941 Earth and Planetary Science Letters, 269(3–4), 576–584. https://doi.org/10.1016/j.epsl.2008.03.016
942 Herrmann, S., & Thierstein, H. R. (2012). Cenozoic coccolith size changes-Evolutionary and/or ecological
943 controls? Palaeogeography, Palaeoclimatology, Palaeoecology, 333–334, 92–106.
944 https://doi.org/10.1016/j.palaeo.2012.03.011

945 Hodel, F., Fériot, C., Dera, G., De Rafélis, M., Lezin, C., Nardin, E., … Chavagnac, V. (2022). Eocene-
946 Oligocene southwest Pacific Ocean paleoceanography new insights from foraminifera chemistry (DSDP
947 site 277, Campbell Plateau). *Frontiers in Earth Science, 10*. https://doi.org/10.3389/feart.2022.998237
948 Hodel, F., Grespan, R., de Rafélis, M., Dera, G., Lezin, C., Nardin, E., … Chavagnac, V. (2021). Drake Passage
949 gateway opening and Antarctic Circumpolar Current onset 31 Ma ago: The message of foraminifera and
950 reconsideration of the Neodymium isotope record. *Chemical Geology, 570,* 120171.
951 https://doi.org/10.1016/j.chemgeo.2021.120171
952 Houben, A. J. P., Van Mourik, C. A., Montanari, A., Coccioni, R., & Brinkhuis, H. (2012). The Eocene-
953 Oligocene transition: Changes in sea level, temperature or both? *Palaeogeography, Palaeoclimatology,*
954 *Palaeoecology*, *335–336*, 75–83. https://doi.org/10.1016/j.palaeo.2011.04.008
955 Houben, A. J. P., Bijl, P. K., Pross, J., Bohaty, S. M., Passchier, S., Stickley, C. E., … Scientists, and the E.
956 318. (2013). Reorganization of Southern Ocean Plankton Ecosystem at the onset of Antarctic Glaciation.
957 *Science*, *340*(6130), 341–344. https://doi.org/10.1126/science.1223646
958 Houben, A. J. P., Bijl, P. K., Sluijs, A., Schouten, S., & Brinkhuis, H. (2019). Late Eocene Southern Ocean
959 Cooling and Invigoration of Circulation Preconditioned Antarctica for Full-Scale Glaciation.
960 *Geochemistry, Geophysics, Geosystems*, *20*, 2214–2234. https://doi.org/10.1029/2019GC008182
961 Hu, J., Gurnis, M., Rudi, J., Stadler, G., & Müller, R. D. (2022). Dynamics of the abrupt change in Pacific
962 Plate motion around 50 million years ago. *Nature Geoscience*, *15*(1), 74–78.
963 https://doi.org/10.1038/s41561-021-00862-6
964 Huber, M., Brinkhuis, H., Stickley, C. E., Döös, K., Sluijs, A., Warnaar, J., … Williams, G. L. (2004). Eocene
965 circulation of the Southern Ocean: Was Antarctica kept warm by subtropical waters?
966 *Paleoceanography*, *19*(PA4026), 1–12. https://doi.org/10.1029/2004PA001014
967 Hutchinson, D. K., Coxall, H. K., Lunt, D. J., Steinthorsdottir, M., de Boer, A. M., Baatsen, M., … Zhang, Z.
968 (2021). The Eocene–Oligocene transition: a review of marine and terrestrial proxy data, models and
969 model–data comparisons. *Climate of the Past*, *17*(1), 269–315. https://doi.org/10.5194/cp-17-269-2021
970 Iglesias-Rodríguez, M. D., Brown, C. W., Doney, S. C., Kleypas, J., Kolber, D., Kolber, Z., … Falkowski, P.
971 G. (2002). Representing key phytoplankton functional groups in ocean carbon cycle models:
972 Coccolithophorids. *Global Biogeochemical Cycles, 16*(4), 1100. https://doi.org/10.1029/2001gb001454
973 Jones, A. P., Dunkley Jones, T., Coxall, H. K., Pearson, P. N., Nala, D., & Hoggett, M. (2019). Low-Latitude
974 Calcareous Nannofossil Response in the Indo-Pacific Warm Pool Across the Eocene-Oligocene
975 Transition of Java, Indonesia. *Paleoceanography and Paleoclimatology, 34*, 1833–1847.
976 https://doi.org/10.1029/2019PA003597
977 Kamp, P. J. J., Waghorn, D. B., & Nelson, C. S. (1990). Late eocene-early oligocene integrated isotope
978 stratigraphy and biostratigraphy for paleoshelf sequences in southern Australia: paleoceanographic
979 implications. *Palaeogeography, Palaeoclimatology, Palaeoecology*, *80*(3–4), 311–323.
980 https://doi.org/10.1016/0031-0182(90)90140-3
981 Katz, M. E., Miller, K. G., Wright, J. D., Wade, B. S., Browning, J. V., Cramer, B. S., & Rosenthal, Y. (2008).
982 Stepwise transition from the Eocene greenhouse to the Oligocene icehouse. *Nature Geoscience*, *1*(5),

329–333. https://doi.org/10.1038/ngeo179

Kennett, J. P. (1977). Cenozoic evolution of Antarctic glaciation, the circum-Antarctic Ocean, and their impact on global paleoceanography. *Journal of Geophysical Research*, *82*(27), 3843–3859. https://doi.org/10.1029/JC082i027p03843

Kennett, J. P. (1978). The development of planktonic biogeography in the Southern Ocean during the Cenozoic. *Marine Micropaleontology*, *3*(4), 301–345. https://doi.org/10.1016/0377-8398(78)90017-8

Kennett, J. P., Burns, R. E., Andrews, J. E., Churkin, M., Davies, T. A., Dumitrica, P., … van der Lingen, G. J. (1972). Australian-Antarctic Continental Drift, Palaeocirculation Changes and Oligocene Deep-Sea Erosion. *Nature Physical Science*, *239*(91), 51–55.

Kennett, J. P., & Exon, N. F. (2004). Paleoceanographic evolution of the Tasmanian Seaway and its climatic implications. *American Geophysical Union Geophysical Monograph Series*, *151*, 345–367. Retrieved from http://doi.wiley.com/10.1029/151GM19%0Apapers3://publication/doi/10.1029/151GM19

Kennett, J. P., Houtz, R. E., Andrews, P. B., Edwards, A. R., Gostin, V. A., Hajós, M., … Perch-nielsen, K. (1975a). Cenozoic paleoceanography in the southwest Pacific Ocean, Antarctic glaciation, and the development of the Circum-Antarctic Current. *Initial Reports of the Deep Sea Drilling Project*, *29*, 1155–1169.

Kennett, J. P., Houtz, R. E., Andrews, P. B., Edwards, A. R., Gostin, V. A., Hajos, M., et al. (1975b). Site 283. *Initial Reports of the Deep Sea Drilling Project*, *29*, 365–402. https://doi.org/10.2973/dsdp.proc.29.110.1975

Kennett, J. P., von der Borch, C., Baker, P. A., Barton, C. E., Boersma, A., Caulet, J. P., et al. (1982). Site 592; Lord Howe Rise; 36°S. *Initial Report Deep Sea Drilling Project*, *90*, 487–550.

Lear, C. H., Bailey, T. R., Pearson, P. N., Coxall, H. K., & Rosenthal, Y. (2008). Cooling and ice growth across the Eocene-Oligocene transition. *Geology*, *36*(3), 251–254. https://doi.org/10.1130/G24584A.1

Lear, C. H., Elderfield, H., & Wilson, P. A. (2000). Cenozoic deep-sea temperatures and global ice volumes from Mg/Ca in benthic foraminiferal calcite. *Science*, *287*, 269–272. https://doi.org/10.1126/science.287.5451.269

Liu, Z., Pagani, M., Zinniker, D., Deconto, R. ., Huber, M., Brinkhuis, H., … Pearson, A. (2009). Global cooling during the Eocene-Oligocene climate transition. *Science*, *323*(5918), 1187–1190. https://doi.org/10.1126/science.1166368

Liu, Z., Tuo, S., Zhao, Q., Cheng, X., & Huang, W. (2004). Deep-water earliest Oligocene glacial maximum (EOGM) in South Atlantic. *Chinese Science Bulletin*, *49*(20), 2190–2197. https://doi.org/10.1360/04wd0228

Livermore, R., Hillenbrand, C. D., Meredith, M., & Eagles, G. (2007). Drake Passage and Cenozoic climate: An open and shut case? *Geochemistry, Geophysics, Geosystems*, *8*(1). https://doi.org/10.1029/2005GC001224

Ma, R., Aubry, M., Bord, D., Jin, X., & Liu, C. (2023). Inferred nutrient forcing on the late middle Eocene to early Oligocene (∼40–31 Ma) evolution of the coccolithophore *Reticulofenestra* (order Isochrysidales). *Paleobiology*, 1–14. https://doi.org/10.1017/ pab.2023.20

MacArthur, R. H., & Wilson, E. O. (1967). The Theory of Island Biogeography.

Martini, E. (1971). Standard Tertiary and Quaternary calcareous nannoplankton zonation. In A. Farinacci (Ed.), Proceedings of the 2nd International Conference on Planktonic Microfossils (pp. 739–785). Rome: Edizioni Tecnoscienza.

Miller, K. G., Wright, J. D., & Fairbanks, R. G. (1991). Unlocking the Ice House: Oligocene-Miocene oxygen isotopes, eustasy, and margin erosion. *Journal of Geophysical Research: Solid Earth*, *96*(B4), 6829–6848. https://doi.org/10.1029/90JB02015

Monechi, S., Buccianti, A., & Gardin, S. (2000). Biotic signals from nannoflora across the iridium anomaly in the upper Eocene of the Massignano section: evidence from statistical analysis. *Marine Micropaleontology*, *39*(1–4), 219–237. https://doi.org/10.1016/S0377-8398(00)00022-0

Moore, T. C., van Andel, T. H., Sancetta, C., & Pisias, N. (1978). Cenozoic Hiatuses in Pelagic Sediments. *Micropaleontology*, *24*(2), 113. https://doi.org/10.2307/1485246

Murphy, M. G., Kennett, J. P., & Island, R. (1986). Development of latitudinal thermal gradients during the Oligocene: oxygen-isotope evidence from the southwest Pacific. *Initial Reports of Deep Sea Drilling Project 90*, 1347–1360.

Nelson, C. S., & Cooke, P. J. (2001). History of oceanic front development in the New Zealand sector of the southern ocean during the cenozoic - A synthesis. *New Zealand Journal of Geology and Geophysics*, *44*(4), 535–553. https://doi.org/10.1080/00288306.2001.9514954

Newsam, C., Bown, P. R., Wade, B. S., & Jones, H. L. (2017). Muted calcareous nannoplankton response at the Middle/Late Eocene Turnover event in the western North Atlantic Ocean. *Newsletters on Stratigraphy*, *50*(3), 297–309. https://doi.org/10.1127/nos/2016/0306

Nooteboom, P. D., Baatsen, M., Bijl, P. K., Kliphuis, M. A., van Sebille, E., Sluijs, A., … von der Heydt, A. S. (2022). Improved Model-Data Agreement With Strongly Eddying Ocean Simulations in the Middle-Late Eocene. Paleoceanography and Paleoclimatology, 37(8), 1–13. https://doi.org/10.1029/2021PA004405

Okada, H., & Bukry, D. (1980). Supplementary modification and introduction of code numbers to the low-latitude coccolith biostratigraphic zonation. Marine Micropaleontology, 5, 321–325. https://doi.org/10.1016/0377-8398(80)90016-X

Oke, P. R., Pilo, G. S., Ridgway, K., Kiss, A., & Rykova, T. (2019). A search for the Tasman Front. *Journal of Marine Systems*, *199*, 103217. https://doi.org/10.1016/j.jmarsys.2019.103217

Oke, P. R., Roughan, M., Cetina-Heredia, P., Pilo, G. S., Ridgway, K. R., Rykova, T., … Vitarelli, E. (2019). Revisiting the circulation of the East Australian Current: Its path, separation, and eddy field. *Progress in Oceanography*, *176*, 102139. https://doi.org/10.1016/j.pocean.2019.102139

Pagani, M., Huber, M., Liu, Z., Bohaty, S. M., Henderiks, J., Sijp, W., … DeConto, R. M. (2011). The role of carbon dioxide during the onset of antarctic glaciation. *Science*, *334*(6060), 1261–1264. https://doi.org/10.1126/science.1203909

Pälike, H., Lyle, M. W., Nishi, H., Raffi, I., Ridgwell, A., Gamage, K., … Zeebe, R. E. (2012). A Cenozoic record of the equatorial Pacific carbonate compensation depth. *Nature*, *488*, 609–614.

https://doi.org/10.1038/nature11360

Pascher, K. M. (2017). *Paleobiogeography of Eocene Radiolarians in the Southwest Pacific (Doctoral dissertation)*. Victoria University of Wellington. Retrieved from https://researcharchive.vuw.ac.nz/.

Pascher, K. M., Hollis, C. J., Bohaty, S. M., Cortese, G., McKay, R. M., Seebeck, H., … Chiba, K. (2015). Expansion and diversification of high-latitude radiolarian assemblages in the late Eocene linked to a cooling event in the southwest Pacific. *Climate of the Past*, *11*(12), 1599–1620. https://doi.org/10.5194/cp-11-1599-2015

Pearson, P. N., Foster, G. L., & Wade, B. S. (2009). Atmospheric carbon dioxide through the Eocene-Oligocene climate transition. *Nature*, *461*(7267), 1110–1113. https://doi.org/10.1038/nature08447

Pearson, P. N., McMillan, I. K., Wade, B. S., Dunkley Jones, T., Coxall, H. K., Bown, P. R., & Lear, C. H. (2008). Extinction and environmental change across the Eocene-Oligocene boundary in Tanzania. *Geology*, *36*(2), 179–182. https://doi.org/10.1130/G24308A.1

Perch-Nielsen, K. (1985). Cenozoic calcareous nannofossils. In H. M. Bolli, J. B. Saunders, & K. Perch-Nielsen (Eds.), *Plankton Stratigraphy* (pp. 427–555). Cambridge: Cambridge University Press.

Persico, D., & Villa, G. (2004). Eocene-Oligocene calcareous nannofossils from Maud Rise and Kerguelen Plateau (Antarctica): Paleoecological and paleoceanographic implications. *Marine Micropaleontology*, *52*(1–4), 153–179. https://doi.org/10.1016/j.marmicro.2004.05.002

Persico, D., & Villa, G. (2008). A new Eocene Chiasmolithus species: hypothetical reconstruction of its phyletic lineage. *Journal of Nannoplankton Research*, *30*(1), 23–33.

Pianka, E. R. (1970). On r- and K-Selection. *The American Naturalist*, *104*(940), 592–597. https://doi.org/10.1086/282697

Reghellin, D. (2019). *Eastern equatorial Pacific bulk sediment properties and paleoceanography since the late Neogene (Doctoral dissertation)*. Stockholm University. Retrieved from https://www.su.se/department-of-geological-sciences/research/publications/lic-and-doctoral-theses-1.555109

Reghellin, D., Coxall, H. K., Dickens, G. R., & Backman, J. (2015). Carbon and oxygen isotopes of bulk carbonate in sediment deposited beneath the eastern equatorial Pacific over the last 8 million years. *Paleoceanography*, *30*(10), 1261–1286. https://doi.org/10.1002/2015PA002825

Ridgway, K. R., & Dunn, J. R. (2003). Mesoscale structure of the mean East Australian Current System and its relationship with topography. *Progress in Oceanography*, *56*(2), 189–222. https://doi.org/10.1016/S0079-6611(03)00004-1

Rintoul, S. R., Hughes, C., & Olbers, D. (2001). The Antarctic Circumpolar Current System. In *International Geophysics* (pp. 271–XXXVI). Academic Press.

Roberts, A. P., Florindo, F., Villa, G., Chang, L., Jovane, L., Bohaty, S. M., … Gerald, J. D. F. (2011). Magnetotactic bacterial abundance in pelagic marine environments is limited by organic carbon flux and availability of dissolved iron. *Earth and Planetary Science Letters*, *310*, 441–452. https://doi.org/10.1016/j.epsl.2011.08.011

Rost, B., & Riebesell, U. (2004). Coccolithophores and the biological pump: responses to environmental

changes. In Hans R. Thierstein & J. R. Young (Eds.), *Coccolithophores - From Molecular Process to Global Impact* (Springer, pp. 99–125). Berlin.

Salamy, K. A., & Zachos, J. C. (1999). Latest Eocene-Early Oligocene climate change and Southern Ocean fertility: Inferences from sediment accumulation and stable isotope data. *Palaeogeography, Palaeoclimatology, Palaeoecology*, *145*(1–3), 61–77. https://doi.org/10.1016/S0031-0182(98)00093-5

Sarkar, S., Basak, C., Frank, M., Berndt, C., Huuse, M., Badhani, S., & Bialas, J. (2019). Late Eocene onset of the Proto-Antarctic Circumpolar Current. *Scientific Reports*, *9*(1), 10125. https://doi.org/10.1038/s41598-019-46253-1

Sauermilch, I., Whittaker, J. M., Bijl, P. K., Totterdell, J. M., & Jokat, W. (2019). Tectonic, Oceanographic, and Climatic Controls on the Cretaceous-Cenozoic Sedimentary Record of the Australian-Antarctic Basin. Journal of Geophysical Research: Solid Earth, 124(8), 7699–7724. https://doi.org/10.1029/2018JB016683

Sauermilch, I., Whittaker, J. M., Klocker, A., Munday, D. R., Hochmuth, K., Bijl, P. K., & LaCasce, J. H. (2021). Gateway-driven weakening of ocean gyres leads to Southern Ocean cooling. *Nature Communications*, *12*(1), 1–8. https://doi.org/10.1038/s41467-021-26658-1

Scher, H. D., Whittaker, J. M., Williams, S. E., Latimer, J. C., Kordesch, W. E. C., & Delaney, M. L. (2015). Onset of Antarctic Circumpolar Current 30 million years ago as Tasmanian Gateway aligned with westerlies. *Nature*, *523*, 580–583. https://doi.org/10.1038/nature14598

Shannon, C. E., & Weaver, W. (1949). *The Mathematical Theory of Communication*. University of Illinois Press, Champaign, IL.

Sijp, W. P., England, M. H., & Huber, M. (2011). Effect of the deepening of the Tasman Gateway on the global ocean. *Paleoceanography*, *26*(PA4207), 1–18. https://doi.org/10.1029/2011PA002143

Sijp, W. P., England, M. H., Sijp, W. P., & England, M. H. (2004). Effect of the Drake Passage Throughflow on Global Climate. *Journal of Physical Oceanography*, *34*, 1254–1266. https://doi.org/10.1175/1520-0485(2004)034<1254:EOTDPT>2.0.CO;2

Spencer-Cervato, C. (1999). The Cenozoic deep sea microfossil record: explorations of the DSDP/ODP sample set using the Neptune database. *Palaeontologia electronica*, *22*(1), 1-268.

Spofforth, D. J. A., Agnini, C., Pälike, H., Rio, D., Fornaciari, E., Giusberti, L., … Muttoni, G. (2010). Organic carbon burial following the middle Eocene climatic optimum in the central western Tethys. *Paleoceanography*, *25*, PA3210. https://doi.org/10.1029/2009PA001738

Stickley, C. E., Brinkhuis, H., Schellenberg, S. A., Sluijs, A., Röhl, U., Fuller, M., … Williams, G. L. (2004). Timing and nature of the deepening of the Tasmanian Gateway. *Paleoceanography*, *19*(4), 1–18. https://doi.org/10.1029/2004PA001022

Sutherland, R., Collot, J., Bache, F., Henrys, S., Barker, D., Browne, G. H., … Stratford, W. (2017). Widespread compression associated with Eocene Tonga-Kermadec subduction initiation. *Geology*, *45*(4), 355–358. https://doi.org/10.1130/G38617.1

Sutherland, R., Dickens, G. R., Blum, P., Agnini, C., Alegret, L., Bhattacharya, J., … Zhou, X. (2019). Site U1509. *Tasman Frontier Subduction Initiation and Paleogene Climate. Proceedings of the International*

Ocean Discovery Program, 371: College Station, TX. https://doi.org/10.14379/iodp.proc.371.106.2019

Sutherland, R., Dickens, G. R., Blum, P., & and the Expedition 371 Scientists. (2018). Expedition 371 Preliminary Report: Tasman Frontier Subduction Initiation and Paleogene Climate. *International Ocean Discovery Program*. https://doi.org/10.14379/iodp.pr.371.2018

Sutherland, R., Dickens, G. R., Blum, P., Agnini, C., Alegret, L., Asatryan, G., et al. (2020). Continental scale of geographic change across Zealandia during Paleogene subduction zone initiation. Geology, 48(5), 419–424. https://doi.org/10.1130/G47008.1

Sutherland, R., Dos Santos, Z., Agnini, C., Alegret, L., Lam, A. R., Westerhold, T., … Asatryan, G. (2022). Neogene Mass Accumulation Rate of Carbonate Sediment Across Northern Zealandia, Tasman Sea, Southwest Pacific. *Paleoceanography and Paleoclimatology*, *37*(2), 1–22. https://doi.org/10.1029/2021PA004294

Tagliabue, A., & Bopp, L. (2008). Towards understanding global variability in ocean carbon-13. *Global* Biogeochemical Cycles, 22(1), 1–13. https://doi.org/10.1029/2007GB003037

Taylor, V. E., Westerhold, T., Bohaty, S. M., Backman, J., Dunkley Jones, T., Edgar, K. M., … Wilson, P. A. (2023). Transient Shoaling, Over-Deepening and Settling of the Calcite Compensation Depth at the Eocene-Oligocene Transition. Paleoceanography and Paleoclimatology, 38(6), 1–15. https://doi.org/10.1029/2022pa004493

Tibbett, E. J., Scher, H. D., Warny, S., Tierney, J. E., Passchier, S., & Feakins, S. J. (2021). Late Eocene record of hydrology and temperature from Prydz Bay, East Antarctica. Paleoceanography and Paleoclimatology, 1–21. https://doi.org/10.1029/2020pa004204

Toffanin, F., Agnini, C., Fornaciari, E., Rio, D., Giusberti, L., Luciani, V., … Pälike, H. (2011). Changes in calcareous nannofossil assemblages during the Middle Eocene Climatic Optimum: Clues from the central-western Tethys (Alano section, NE Italy). Marine Micropaleontology, 81(1–2), 22–31. https://doi.org/10.1016/j.marmicro.2011.07.002

Tozzi, S., Schofield, O., & Falkowski, P. (2004). Historical climate change and ocean turbulence as selective agents for two key phytoplankton functional groups. *Marine Ecology Progress Series*, 274, 123–132. https://doi.org/10.3354/meps274123

Tremolada, F., & Bralower, T. J. (2004). Nannofossil assemblage fluctuations during the Paleocene-Eocene Thermal Maximum at Sites 213 (Indian Ocean) and 401 (North Atlantic Ocean): palaeoceanographic implications. *Marine Micropaleontology*, *52*, 107–116. https://doi.org/10.1016/j.marmicro.2004.04.002

Vernet, M., Geibert, W., Hoppema, M., Brown, P. J., Haas, C., Hellmer, H. H., … Verdy, A. (2019). The Weddell Gyre, Southern Ocean: Present Knowledge and Future Challenges. *Reviews of Geophysics*, *57*(3), 623–708. https://doi.org/10.1029/2018RG000604

Viganò, A., Coxall, H. K., Holmström, M., Vinco, M., Lear, C. H., & Agnini, C. (2023a). Calcareous nannofossils across the Eocene-Oligocene transition at Site 756 (Ninetyeast Ridge, Indian Ocean): implications for biostratigraphy and paleoceanographic clues. *Newsletters on Stratigraphy*, *56*(2), 187–223. https://doi.org/10.1127/nos/2022/0725

Viganò, A., Dallanave, E., Alegret, L., Westerhold, T., Sutherland, R., Dickens, G. R., … Agnini, C. (2024a).

Calcareous nannofossil biostratigraphy and biochronology across the Eocene-Oligocene transition: the record at IODP Site U1509 (Tasman Sea) and a global overview. *Newsletters on Stratigraphy*, *57*(1). https://doi.org/10.1127/nos/2023/0751

Viganò, Allyson; Dallanave, Edoardo; Alegret, Laia; Westerhold, Thomas; Sutherland, Rupert; Dickens, Gerald Roy; Newsam, Cherry; Agnini, Claudia (2024b). Calcareous nannofossil data from IODP Site 371-U1509. [Dataset], PANGAEA, https://doi.org/10.1594/PANGAEA.963607

Viganò, Allyson; Dallanave, Edoardo; Alegret, Laia; Westerhold, Thomas; Sutherland, Rupert; Dickens, Gerald Roy; Newsam, Cherry; Agnini, Claudia (2024c). Stable isotope data from IODP Site 371-U1509. [Dataset], PANGAEA, https://doi.org/10.1594/PANGAEA.963608

Viganò, A., Westerhold, T., Bown, P. R., Dunkley Jones, T., & Agnini, C. (2023b). Calcareous nannofossils across the Eocene-Oligocene transition: Preservation signals and biostratigraphic remarks from ODP Site 1209 (NW Pacific, Shatsky Rise) and IODP Hole U1411B (NW Atlantic Ocean, Newfoundland Ridge). *Palaeogeography, Palaeoclimatology, Palaeoecology*, *629*, 111778. https://doi.org/10.1016/j.palaeo.2023.111778

Villa, G., Fioroni, C., Pea, L., Bohaty, S. M., & Persico, D. (2008). Middle Eocene-late Oligocene climate variability: Calcareous nannofossil response at Kerguelen Plateau, Site 748. *Marine Micropaleontology*, *69*, 173–192. https://doi.org/10.1016/j.marmicro.2008.07.006

Villa, G., Fioroni, C., Persico, D., Roberts, A. P., & Florindo, F. (2014). Middle Eocene to Late Oligocene Antarctic glaciation/deglaciation and Southern Ocean productivity. *Paleoceanography*, *29*(3), 223–237. https://doi.org/10.1002/2013PA002518

Villa, G., Florindo, F., Persico, D., Lurcock, P., de Martini, A. P., Jovane, L., & Fioroni, C. (2021). Integrated calcareous nannofossil and magnetostratigraphic record of ODP Site 709: Middle Eocene to late Oligocene paleoclimate and paleoceanography of the Equatorial Indian Ocean. *Marine Micropaleontology*, *169*, 102051. https://doi.org/10.1016/j.marmicro.2021.102051

Wade, B. S., & Bown, P. R. (2006). Calcareous nannofossils in extreme environments: the Messinian Salinity Crisis, Polemi Basin, Cyprus. *Palaeogeography, Palaeoclimatology, Palaeoecology*, *233*, 271–286. https://doi.org/10.1016/j.palaeo.2005.10.007

Wade, B. S., & Pearson, P. N. (2008). Planktonic foraminiferal turnover, diversity fluctuations and geochemical signals across the Eocene/Oligocene boundary in Tanzania. *Marine Micropaleontology*, *68*(3–4), 244–255. https://doi.org/10.1016/j.marmicro.2008.04.002

Wade, B. S., Pearson, P. N., Berggren, W. A., & Pälike, H. (2011). Review and revision of Cenozoic tropical planktonic foraminiferal biostratigraphy and calibration to the geomagnetic polarity and astronomical time scale. Earth-Science Reviews, 104(1–3), 111–142. https://doi.org/10.1016/j.earscirev.2010.09.003

Wei, W., & Wise, S. W. (1990). Biogeographic gradients of middle Eocene-Oligocene calcareous nannoplankton in the South Atlantic Ocean. *Palaeogeography, Palaeoclimatology, Palaeoecology*, *79*, 29–61. https://doi.org/10.1016/0031-0182(90)90104-F

Whittaker, R. H. (1972). Evolution and Measurement of Species Diversity. Taxon, 21, 213–251.

Winter, Amos, Jordan, R. W., & Roth, P. H. (1994). Biogeography of living coccolithophores in ocean waters.

In A. Winter & W. G. Siesser (Eds.), *Coccolithophores* (pp. 161–177). Cambridge: Cambridge University Press.

Young, J. R. (1990). Size variation of Neogene *Reticulofenestra* coccoliths from Indian Ocean DSDP Cores. *Journal of Micropalaeontology*, *9*(1), 71–85. https://doi.org/10.1144/jm.9.1.71

Zachos, J. C., & Kump, L. R. (2005). Carbon cycle feedbacks and the initiation of Antarctic glaciation in the earliest Oligocene. *Global and Planetary Change*, *47*, 51–66. https://doi.org/10.1016/j.gloplacha.2005.01.001

Zachos, J. C., Pagani, M., Sloan, L., Thomas, E., & Billups, K. (2001). Trends, Global Rhythms, and Aberrations in Global Climate 65 Ma to Present. *Science*, *292*, 686–693. https://doi.org/10.1126/science.1059412

Zachos, J. C., Stott, L. D., & Lohmann, K. C. (1994). Evolution of Early Cenozoic marine temperatures. *Paleoceanography*, *9*(2), 353–387. https://doi.org/10.1029/93PA03266

Zachos, J. C., Quinn, T. M., & Salamy, K. A. (1996). High-resolution (10^4 years) deep-sea foraminiferal stable isotope records of the Eocene-Oligocene climate transition. *Paleoceanography*, *11*(3), 251–266.

Figure captions

Figure 1 (a) Study interval at Hole U1509A: depth (m, CSF-A), epoch, core, recovery, image, and lithology (Subunit Ic - calcareous chalk and limestone with biosilica and chert) are reported; (b) Present day location of Site U1509 (black star) and other Exp. 371 Sites (U1508-1511) are reported (white stars) in the Southwest Pacific. White circles = relevant DSDP and ODP sites (modified from Sutherland et al., 2018); (c) Polar-centered paleogeographic reconstruction at 34 Ma (modified from Viganò et al., 2024a). Arrows represents cooler (blue) and warmer (red) oceanic currents, as synthetized by Hodel et al. (2022) and compared with recent findings from Sauermilch et al. (2021) and Nooteboom et al. (2022). The approximate position of the pSTF is inferred from Nelson and Cooke (2001). Site U1509 (this study) and Site 756 (Viganò et al., 2023a) (used for comparison) are reported. pACC: proto-Antarctic Circumpolar Current; pTF: proto-Tasman Front; pSTF: proto-Subtropical Front; EAC: East Australian Current; pRG: proto-Ross Gyre; TG: Tasman Gateway; DP: Drake Passage; pWG: proto-Weddell Gyre; pIOG: proto-Indian Ocean Gyre.

Figure 2 Relative abundances (%) of the main components of the calcareous nannofossil assemblages at Site U1509. To the right, percentage of reworking and number of reworked specimens (n) in 1 mm^2. To the left, depth (CSF-A, m), recovery (Sutherland et al., 2019), magnetostratigraphy, calcareous nannofossil biozonations (CP Zone: Okada & Bukry, 1980; NP Zone: Martini, 1971; CN Zone: Agnini et al., 2014), planktonic foraminifera biostratigraphy (E Zone: Wade et al., 2011) and chronostratigraphy. Other nannofossil genera (%) discussed in the main text are provided in the Supporting Information (Figure S1).

Figure 3 Additional relative abundances (%) of formal and informal (size) groups belonging to calcareous nannofossil genera *Reticulofenestra* and *Dictyococcites* at Site U1509.

Figure 4 Synthesis of the featured calcareous nannofossil genera (%) along with bulk carbon and oxygen stable isotope and carbonate (%) records at Site U1509. Different colored bands highlight the four intervals in which calcareous nannofossils show significant abundance variations. To the left: depth (m, CSF-A), core and

1249 recovery (Sutherland et al., 2019), magnetostratigraphy, calcareous nannofossil (CN) Zone (Agnini et al.,
1250 2014) and chronostratigraphy. Bulk stable O and C isotopes and carbonate content (%) are shown with a 5-
1251 point running average.

1252 **Figure 5** Bulk stable isotopes (oxygen and carbon) and carbonate content (%) from IODP U1509 versus
1253 magnetostratigraphy, chronostratigraphy, calcareous nannofossil (CN) Zone (Agnini et al., 2014) and related
1254 EOT terminology. Tie-points are available Chron boundaries (Viganò et al., 2024a) calibrated to the GTS20
1255 timescale (Gradstein et al., 2020).

1256 **Figure 6** Warm oligotrophic taxa (%), cold eutrophic taxa (%), quantitative diversity indices (number of
1257 taxa, dominance, Shannon index and evenness), PC1 and PC2 scores, and geochemical data are plotted against
1258 core and recovery (Sutherland et al., 2019), magnetostratigraphy, calcareous nannofossil (CN) Zone (Agnini
1259 et al., 2014) and chronostratigraphy. PC1 and PC2 scores here refers to CN genera data (%). All plots are
1260 shown with a 5-point running average, except for PC1 and PC2 scores. The main paleoenvironmental phases
1261 are also reported.

1262 **Figure 7** Principal component analysis (PCA) plot of placoliths (%) from IODP Site U1509 in terms of the
1263 first and second component (PC1 and PC2). Placoliths are subdivided into 18 taxa.

1264

1265

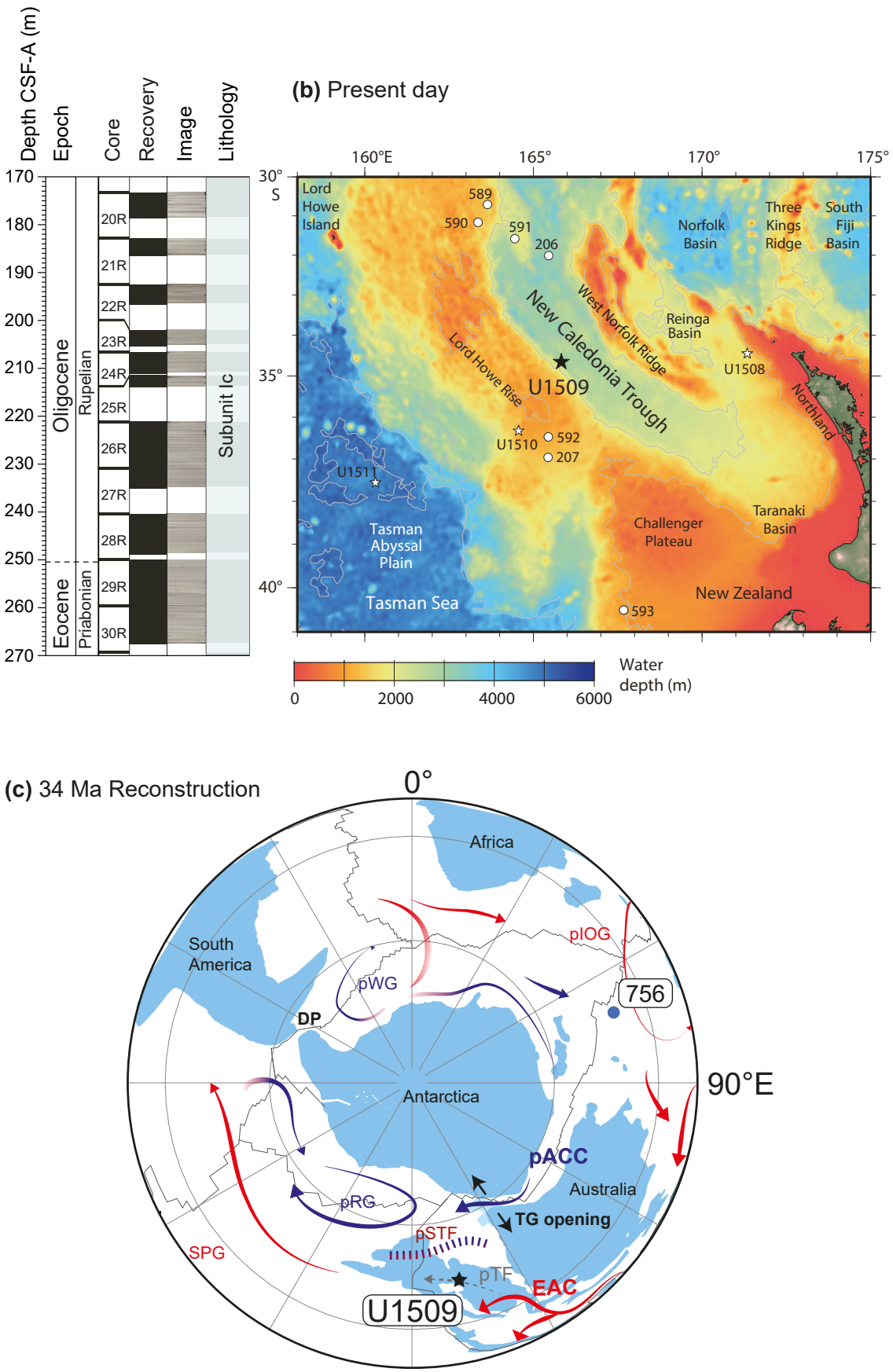
(a) Hole U1509A
Depth CSF-A (m)
Epoch
Core
Recovery
Image
Lithology
170
180
190
200
210
220
230
240
250
260
270
Oligocene
Rupelian
Eocene
Priabonian
20R
21R
22R
23R
24R
25R
26R
27R
28R
29R
30R
Subunit Ic
(b) Present day
160°E
165°
170°
175°
30° S
35°
40°
Lord Howe Island
589
590
591
206
Norfolk Basin
Three Kings Ridge
South Fiji Basin
West Norfolk Ridge
Reinga Basin
New Caledonia Trough
Lord Howe Rise
U1509
U1508
Northland
U1510
592
207
U1511
Tasman Abyssal Plain
Challenger Plateau
Taranaki Basin
Tasman Sea
New Zealand
593
0
2000
4000
6000
Water depth (m)
(c) 34 Ma Reconstruction
0°
Africa
South America
pIOG
pWG
DP
756
90°E
Antarctica
pACC
Australia
pRG
TG opening
pSTF
SPG
pTF
EAC
U1509

Depth CSF-A (m)
Recovery
Polarity Chron
CP Zone
NP Zone
CN Zone
E Zone
Epoch
G. index
Eocene
Oligocene
no data
C15n
C13r
C13n
C12r
15b
16a
16b
16c
17
19/20
21
22
23
E19
E20
E21
O1
O2
O3
15
16
Reticulofenestra
Coccolithus
Dictyococcites
Chiasmolithus
Cyclicargolithus
Clausicoccus
Ericsonia
Isthmolithus
Lanternithus
Discoaster
Reworking
%
Increase of reworking
n/mm²

Depth CSF-A (m)
Recovery
Polarity Chron
CP Zone
NP Zone
CN Zone
E Zone
Epoch
Reticulofenestra
Dictyococcites
%
Reticulofenestra <4 µm
Reticulofenestra 4-10 µm
Reticulofenestra 10-14 µm
Reticulofenestra daviesii
Reticulofenestra umbilicus >14 µm
Dictyococcites 4-10 µm
Dictyococcites 10-14 µm
D. bisectus >10 µm
D. cf. bisectus <10 µm
Dictyococcites filewiczii
Dictyococcites hesslandii
no data
G. index
Eocene
Oligocene

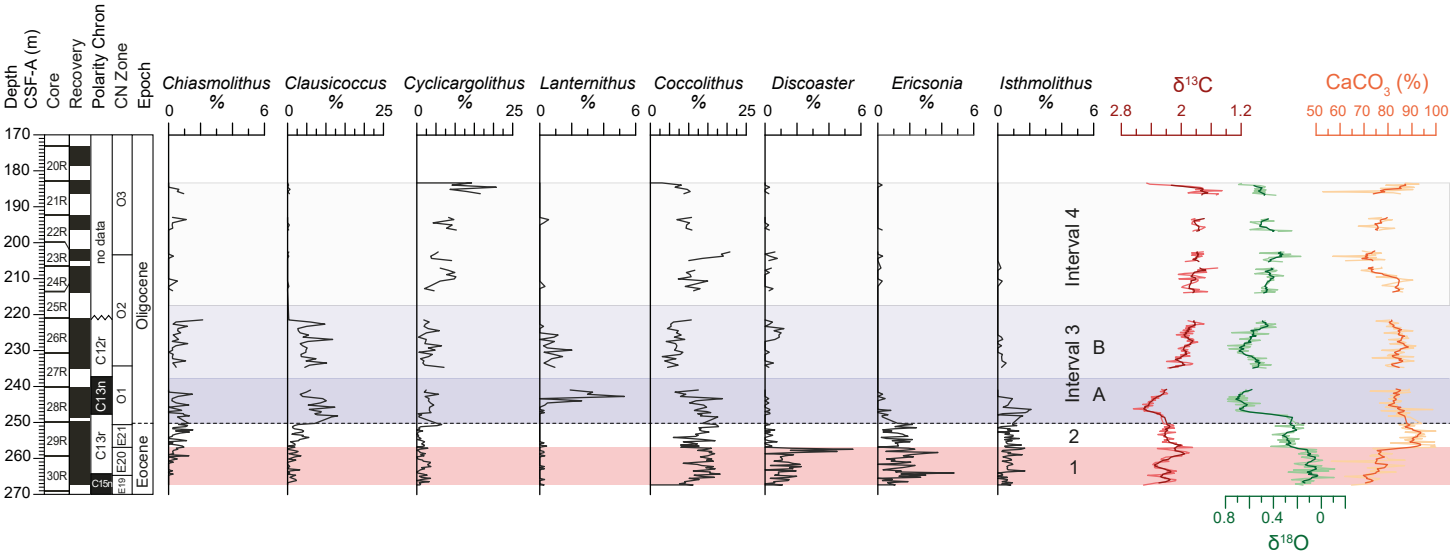
Depth CSF-A (m)
Core
Recovery
Polarity Chron
CN Zone
Epoch
Chiasmolithus
Clausicoccus
Cyclicargolithus
Lanternithus
Coccolithus
Discoaster
Ericsonia
Isthmolithus
%
δ13C
CaCO3 (%)
Interval 4
Interval 3
B
A
2
1
δ18O
no data
Oligocene
Eocene

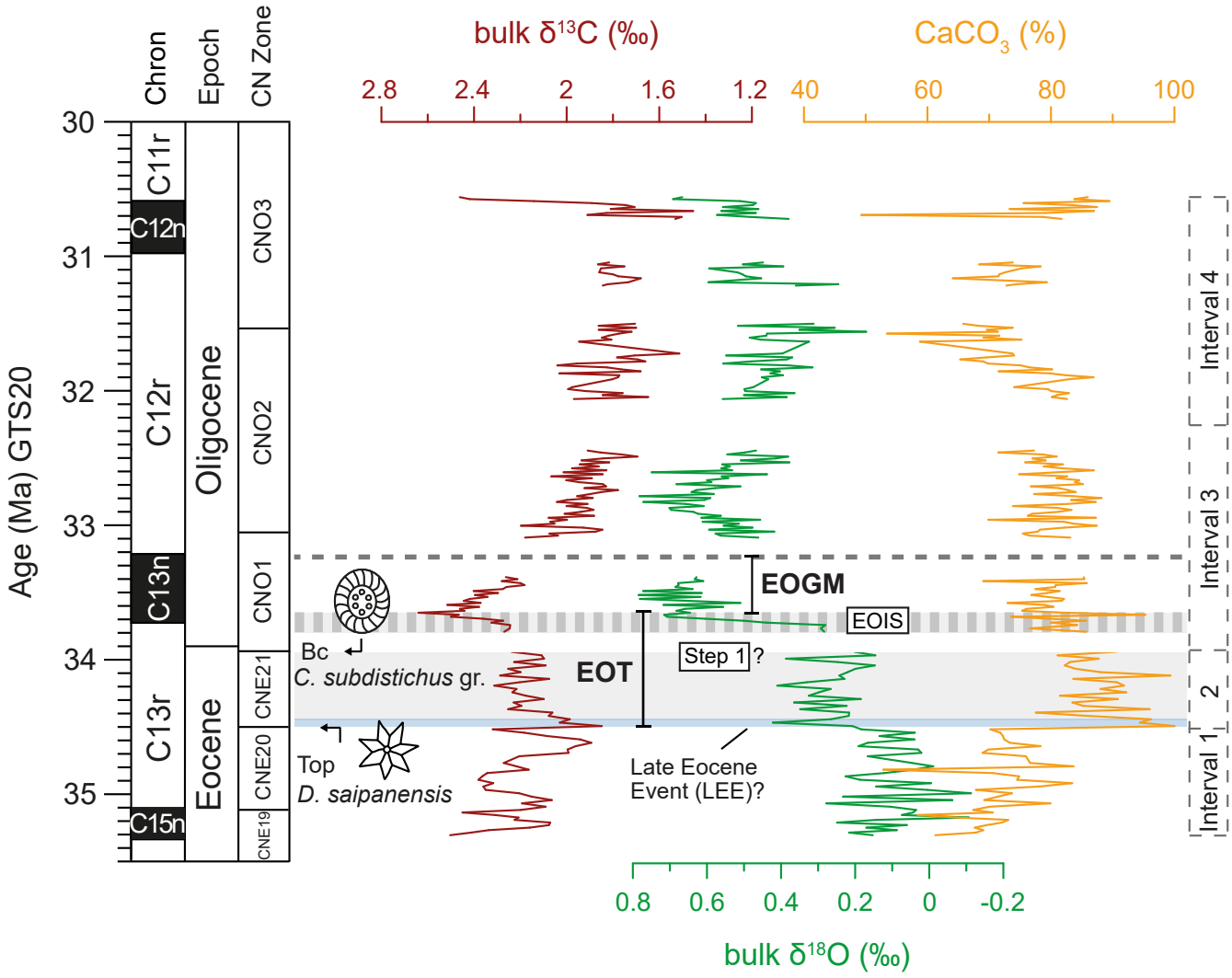
Chron
Epoch
CN Zone
Age (Ma) GTS20
30
31
32
33
34
35
C11r
C12n
C12r
C13n
C13r
C15n
Oligocene
Eocene
CNO3
CNO2
CNO1
CNE21
CNE20
CNE19
bulk δ13C (‰)
2.8
2.4
2
1.6
1.2
CaCO3 (%)
40
60
80
100
Interval 4
Interval 3
Interval 2
Interval 1
EOGM
EOIS
EOT
Step 1?
Bc
C. subdistichus gr.
Top
D. saipanensis
Late Eocene
Event (LEE)?
0.8
0.6
0.4
0.2
0
-0.2
bulk δ18O (‰)

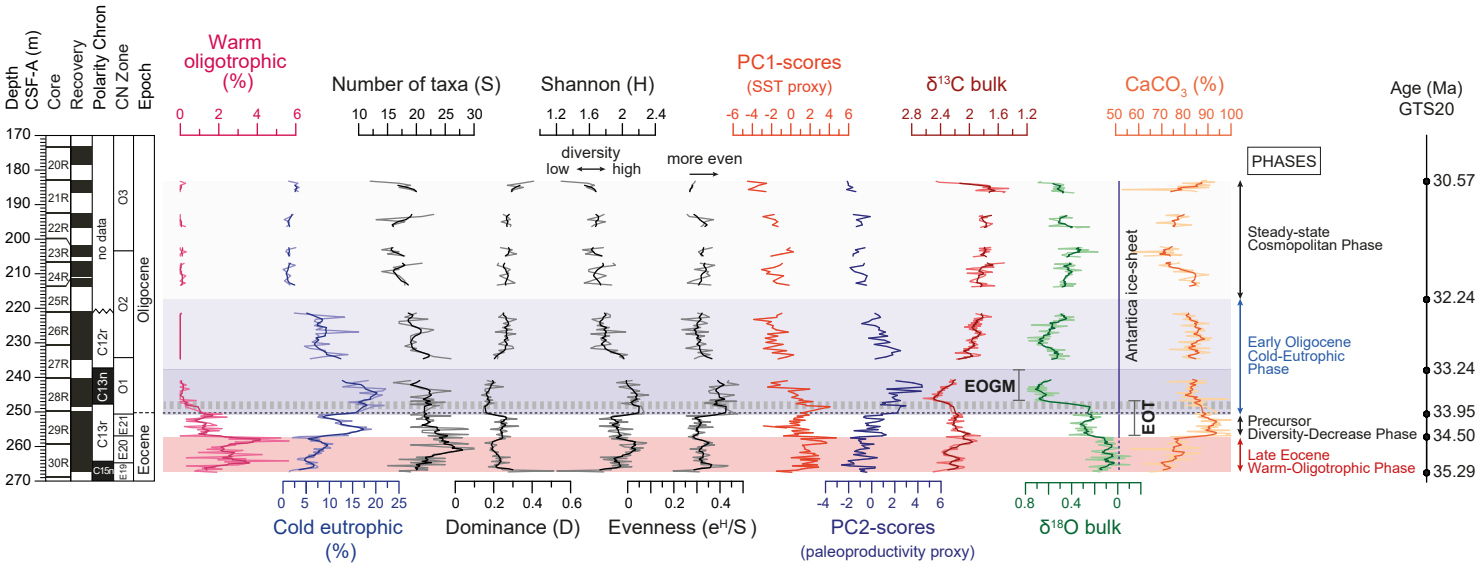
Depth CSF-A (m)
Core
Recovery
Polarity Chron
CN Zone
Epoch
Warm oligotrophic (%)
Number of taxa (S)
Shannon (H)
diversity low ⟷ high
more even
PC1-scores (SST proxy)
δ13C bulk
CaCO3 (%)
Age (Ma) GTS20
PHASES
Steady-state Cosmopolitan Phase
Early Oligocene Cold-Eutrophic Phase
Precursor Diversity-Decrease Phase
Late Eocene Warm-Oligotrophic Phase
Antarctica ice-sheet
EOGM
EOT
Cold eutrophic (%)
Dominance (D)
Evenness (eH/S)
PC2-scores (paleoproductivity proxy)
δ18O bulk
Oligocene
Eocene
no data
30.57
32.24
33.24
33.95
34.50
35.29

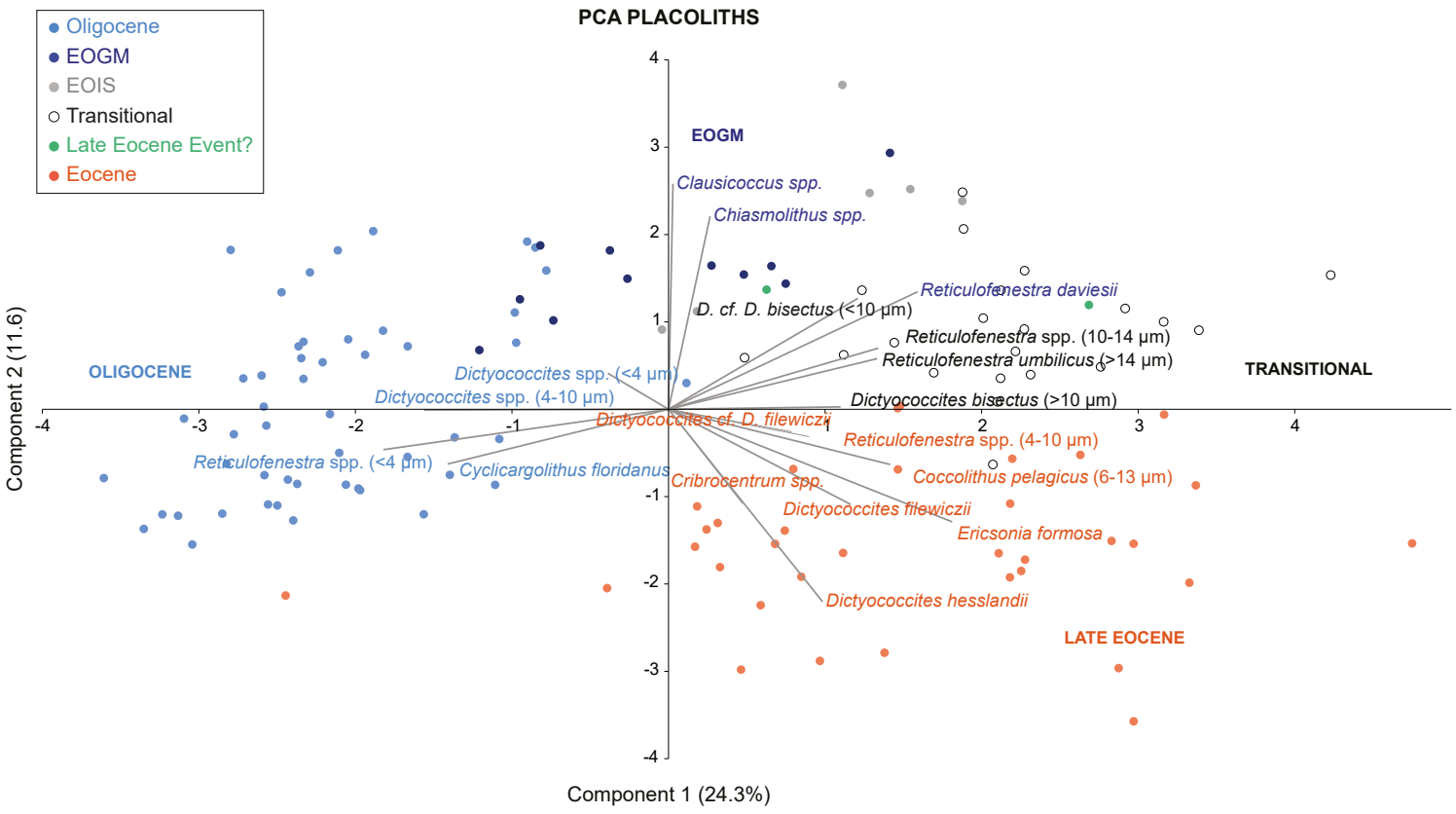
PCA PLACOLITHS
Oligocene
EOGM
EOIS
Transitional
Late Eocene Event?
Eocene
EOGM
Clausicoccus spp.
Chiasmolithus spp.
Reticulofenestra daviesii
D. cf. D. bisectus (<10 µm)
Reticulofenestra spp. (10-14 µm)
Reticulofenestra umbilicus (>14 µm)
TRANSITIONAL
OLIGOCENE
Dictyococcites spp. (<4 µm)
Dictyococcites spp. (4-10 µm)
Dictyococcites bisectus (>10 µm)
Dictyococcites cf. D. filewiczi
Reticulofenestra spp. (4-10 µm)
Reticulofenestra spp. (<4 µm)
Cyclicargolithus floridanus
Cribrocentrum spp.
Coccolithus pelagicus (6-13 µm)
Dictyococcites filewiczii
Ericsonia formosa
Dictyococcites hesslandii
LATE EOCENE
Component 2 (11.6)
Component 1 (24.3%)